Physica D 34 (1989) 1–41
North-Holland, Amsterdam

PATTERN DYNAMICS IN SPATIOTEMPORAL CHAOS

PATTERN SELECTION, DIFFUSION OF DEFECT AND PATTERN COMPETITION INTERMITTENCY

Kunihiko KANEKO
Institute of Physics, College of Arts and Sciences, University of Tokyo, Komaba, Meguro-ku, Tokyo 153, Japan and Center for Complex Systems Research, University of Illinois at Urbana-Champaign, Champaign, IL 61820, USA*

Received 30 December 1987
Revised manuscript received 20 August 1988
Communicated by A.C. Newell

A class of coupled map lattices is investigated as a model for the spatiotemporal chaos. As the parameters are changed, phase transitions among the patterns are observed. Pattern selection through the chaotic motion of domain is observed. Chaos is suppressed by the selection. Selection of the zigzag pattern is studied, where localized defects which separate the two anti-phase domains are found. They change chaotically in time and move randomly in space. The diffusion of defect is related with its chaotic motion. Collapse of zigzag pattern and the defect turbulence are studied in connection with the crisis in high-dimensional dynamical systems. Pattern selection with longer wavelengths is found in the stronger coupling regime. Transition from pattern selection phase to fully developed turbulence occurs via the intermittency. Selective flicker-like noise and the Pareto distribution of lifetime of pattern are observed at the intermittency regime. For the quantitative characterization of each phase, pattern distributions, pattern transition matrix, static and dynamical entropies, lifetime distribution of pattern, spatiotemporal power spectra, and Lyapunov spectra are calculated. Phase transition from the pattern selection to fully developed turbulence is investigated with the use of these quantifiers, where some order parameters and critical indices are introduced.

Contents

*Permanent address.

1. Introduction

Characterization of complex dynamics is one of the most challenging problems in the nonlinear science of our age. Chaos with low degrees of freedom has opened the study towards this direction. The study has shed some light on the understanding of the onset of turbulence and complex dynamics with small degrees of relevant freedom. Most complex dynamics, however, is not governed by small numbers of degrees of freedom, as is seen in the turbulence in a wide sense, observed not only in fluids, but also in optics, solid-state physics, chemistry, and in coupled dynamical systems in biology and technology [1]. For the study of these systems, we have to use a model with time and space.

There already exists many models and simulations towards this approach, such as partial differential equations, lattice differential equations, cellular automata [2], and coupled map lattices [3–5]. Here we use coupled map lattice models for the study of spatiotemporal chaos. See [5] for the discussion on the merit and demerit for each model.

The reason we use a coupled map lattice model (CML) here is as follows: (i) Some notions of dynamical systems theory can be used in the study of CML, and it may also be possible to extend the dynamical systems theory to include the "space". It is also possible to use the notions of information theory, entropies, and Lyapunov analysis, which are utilized in the study of chaos in low-dimensional dynamical systems theory. (ii) CML gives the most convenient and fastest tool for simulation on the computers with floating-point processors, and is especially useful in the parallel computers. By a suitable modelling it can afford a faster tool for some physical simulations as is verified by Oono and Puri [10] for the kinetic Ising or TDGL model. (iii) The model includes continuous parameters and the study of a change of spatiotemporal patterns with the parameter change becomes possible. Since the computation is fast, we can check the global phase diagram. (iv) Statistical mechanics of spin systems on a lattice has made a large progress in the past forty years. Wilson [6] has proposed the lattice gauge theory on the basis of the renormalization group. Here we introduce a lattice chaos model anticipating the future appearance of "lattice chaos theory". We can use some notions, such as critical phenomena, phase transitions, and order parameters corresponding to some patterns, which are developed in the study of spin systems on a lattice.

A coupled map lattice is a dynamical system with a discrete time, discrete space, and continuous state [3, 5, 7, 8], see also [11–14]. Though there are various kinds of the above models, we restrict ourselves only to the following diffusive coupling case here:

$$x_{n+1}(i) = (1-\epsilon) f(x_n(i)) + \epsilon/2\left[f(x_n(i+1)) + f(x_n(i-1)) \right], \tag{1}$$

where n is a discrete time step and i is a lattice point ($i = 1, 2, \ldots, N$ = system size) with a periodic boundary condition. Here the mapping function $f(x)$ is chosen mainly to be the logistic map

$$f(x) = 1 - ax^2, \tag{2}$$

but the phenomena to be shown later can be seen in a wide class of mappings and in other types of couplings. The logistic map (1.1) shows the accumulation of period-doubling at $a = 1.40155\ldots$, and the band merging from period-2 band to a single band state at $a = 1.542\ldots$.

Some results on the coupled map lattice have already been published. In the present paper, we focus on the pattern dynamics in the spatiotemporal chaos.

2. Visualization of phases

In the present section, a "zoo" of coupled map lattice is shown. As methods for visualization, (1)

space–amplitude plots, (2) spatial return maps, and (3) space–time diagram are used. See [5] for the definition and merits of these visualization techniques.

The global phase diagram is given in fig. 1, which was obtained by the simulation from random initial configurations. The meaning of each phase in the figure is explained in the course of the paper. Some examples of the space amplitude plots are shown in figs. 2 and 3, where some typical examples of the pattern of each phase are seen. Also, examples of space–time diagrams are given in figs 4 and 5.

Let us briefly survey the results of the model, and explain the characteristic property of each phase.

2.1. *Frozen random pattern*

As has already been reported, the coupled map lattice model (1) shows the period-doubling of kink–antikinks with the increase of the nonlinearity a [8, 5]. By the doublings, domains of various sizes are formed. After some numbers of doublings, the system exhibits a chaotic behavior at some large domains. The domain boundary does not move in the space and the motion in a domain can be chaotic.

As is seen in the phase diagram (fig. 1), the single logistic map is in the two-band region at the parameter region for this phase. The domain separation is assured by this band splitting.

At this phase, the distribution of domain size depends on the choice of initial conditions. The dynamical state in a domain largely depends on the domain size, as are seen e.g., in figs. 2(a) and 3(a). In a large domain, the motion is quite chaotic, while it is almost period-8 at smaller domain, period-4 for much smaller domains, and period-2 for the smallest ones.

The patterns are fixed in time. If we start from a random initial condition, the pattern of attractor is random in space and depends on the initial condition. Examples of the coexistence of many attractors of different patterns are shown in figs. 6, where the attractors of randomly chosen 10 initial

Table I
List of notations of quantifiers, parameters, and exponents.

$Q(k)$	pattern distribution function
S_p	(static) pattern entropy
S_d	pattern dynamical entropy
$W_k(n)$	lifetime distribution of pattern
t_{lf}	(average) lifetime of a pattern
$T(j \to k)$	pattern transition matrix
$S(k)$	spatial power spectra
$P(k, \omega)$	spatiotemporal power spectra (dynamical form factor)
D	diffusion coefficient of a defect
$\lambda(i)$	Lyapunov spectra
h	KS entropy density
a	bifurcation parameter for the logistic map $1 - ax^2$
ϵ	strength of coupling
N	system size
a_c	onset value of the collapse of pattern
α	$P(k_1, \omega) \propto \omega^{-\alpha}$; selective flicker-like noise[a]
β	$(1 - Q(p_1)) \propto (a - a_c)^{\beta}$; onset of the collapse of pattern[a]
β'	$S_p \propto (a - a_c)^{\beta'}$; onset of the collapse of pattern
δ	$S_d \propto (a - a_c)^{\delta}$; onset of the collapse of pattern
ψ	$W_{p_1}(n) \propto n^{-\psi}$; Pareto–Zipf law[a]

[a] k_1 and p_1 are wavelength(s) and domain size(s) of selected pattern(s).

conditions are depicted. The domain structures in the figure are fixed in space. In the figure, initial conditions are only arbitrarily chosen, but they all are found to belong to basins of different attractors.

The independence of domains leads to the conclusion that the possible number of attractors increases exponentially as system size.

These three features ((1) frozen pattern (2) spatially random attractor for arbitrary chosen random initial configuration, (3) the number of attractors increase exponentially with a system size) are common with the "glassy phase" in solid-state and statistical physics.

2.2. *Pattern selection and suppression of chaos*

As the nonlinearity is increased further, some domain boundaries start to move. Thus the initial

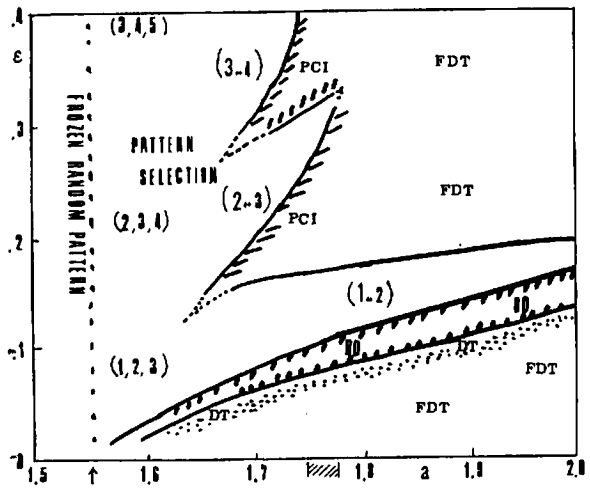

Fig. 1. Phase diagram of the coupled logistic lattice (1): The phases are determined by the spatiotemporal patterns and the distribution function of pattern $Q(k)$ to be defined later. Simulation has been carried out for (1) with random initial configurations and $N = 100$. The parameters are changed from $a = 1.5$ to 2.0 by 0.01 and $\epsilon = 0.02$ to 0.4 by 0.02. Here BD, DT, PCI, and FDT are the abbreviations of Brownian motion of Defect, Defect Turbulence, Pattern Competition Intermittency, and Fully Developed Turbulence, respectively, which are discussed in detail later. The numbers such as 1, 2, 3 represent the selected domain sizes. See text for details. The arrow at the bottom line shows the band merging point for the single logistic map, while the region with oblique lines correspond to the period-3 window in the logistic map.

condition is not preserved anymore. Through the motion of domain boundaries, domains of some special sizes are selected. Some examples of the selection of the patterns are shown in figs. 2(b, c) and 3(b, c). As the nonlinearity is increased, the number of possible patterns decreases and at medium nonlinearity, only 1–3 patterns are selected. The size of the selected domain depends on the value of coupling. The selected size of domain is such that the motion in the domain of the size is less chaotic, i.e., the motion with shorter periods. In the frozen pattern phase, chaos is suppressed only in some domains (with small sizes). Here, the ratio of such domains is increased by the selection.

For examples, compare fig. 2(a) or 3(a) with 2(b) or 3(b, c). In figs. 2(a) and 3(a), chaotic behavior is clearly seen in large domains, while such fully chaotic motion is suppressed in figs. 2(b) and 3(b, c). In fig. 2(b), the dominant structure is the domain size = 1, or in other words, "zigzag structure". Note that the temporal motion of this domain is almost period-2, a very simple temporal motion. In fig. 3(b), the dominant selected patterns are domain size = 2 or 3. In the domain of size = 2, the temporal motion is almost period-2, while in the domain size = 3, it is almost period-4. The "almost" period-K here means the periodic motion of period K with a chaotic modulation of very small amplitude. We also note that the suppression of chaos is stronger in fig. 2(c) than in 2(b). These give the examples for the above statement that the selection occurs in favor of a simple temporal motion.

A precise definition which distinguishes the frozen random state from a pattern selection is given by the following:

In a frozen random state there exists an arbitrary large domain if the system size goes infinity, while there exists a critical size l_c, such that a domain of the size larger than l_c cannot exist.

The phenomena here may be regarded as the suppression of chaos by the diffusion process. The diffusion term has the tendency to produce the homogeneity in space, while the chaotic motion makes the system inhomogeneous due to the sensitive dependence on initial conditions. These two

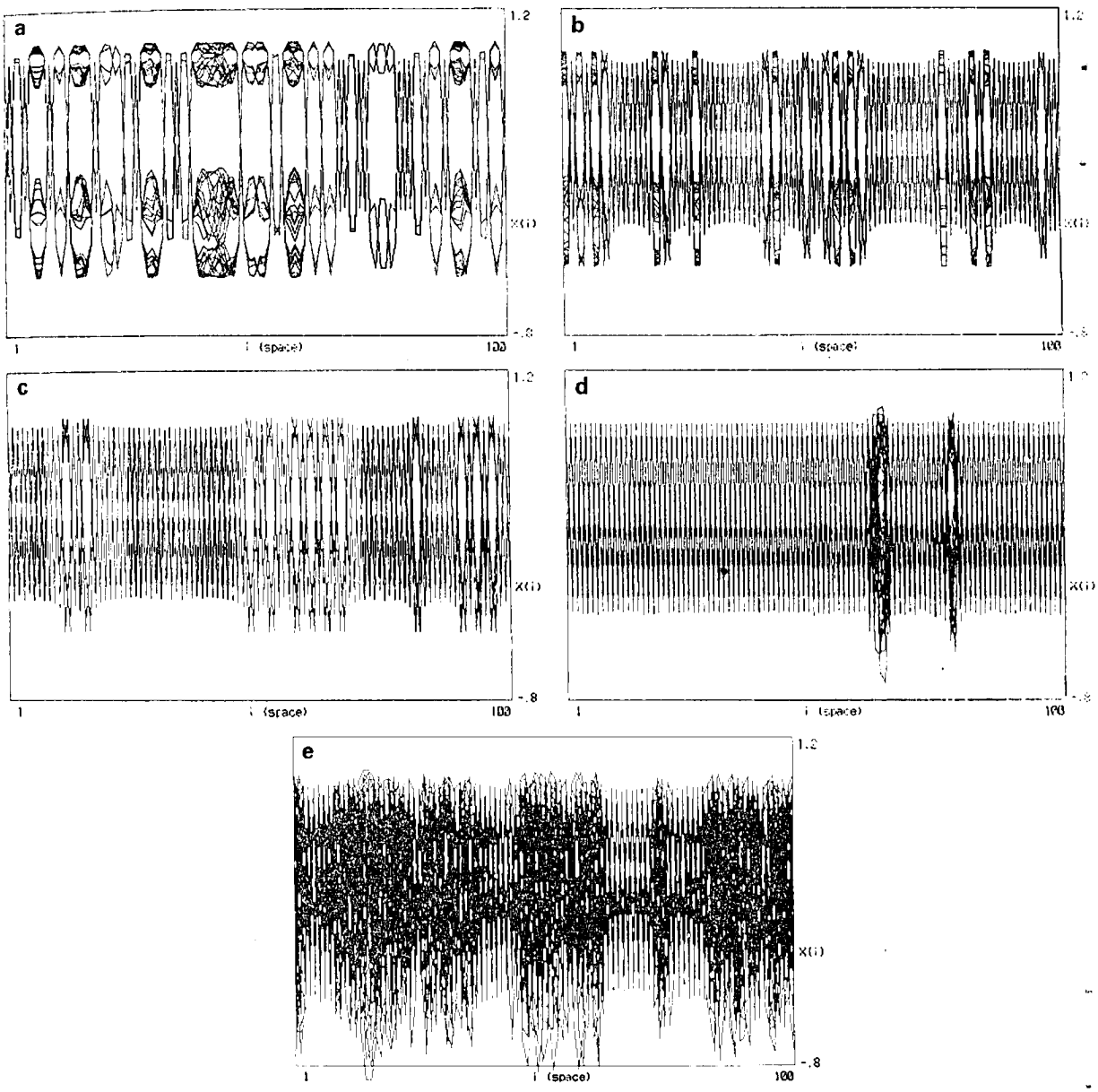

Fig. 2. Space–amplitude plot for the coupled logistic lattice (1). Amplitudes $x_n(i)$'s are overlayed for 50 time steps after the 1000 iterations of transients for the model with $\epsilon = 0.1$, $N = 100$, and random initial configurations. (a) $a = 1.44$, (b) $a = 1.64$ (c) $a = 1.72$: In (a)–(c), domain structures do not move in space. (d) $a = 1.80$: The zigzag region is temporally quasiperiodic, while the defects move around in space. After more iterations they will disappear by collisions. (e) $a = 1.90$.

tendencies conflict with each other. The conflict leads to the splitting of a larger domain. (One may regard this as the splitting by the "chaos pressure".) On the other hand, there is no conflict in the domains of almost periodic motion, where a cancellation of the above two tendencies leads to a simple pattern. In this sense, we may term the present phase as "pattern selection through transient chaos and diffusion". After the selection, the pattern of domains is fixed and does not move in

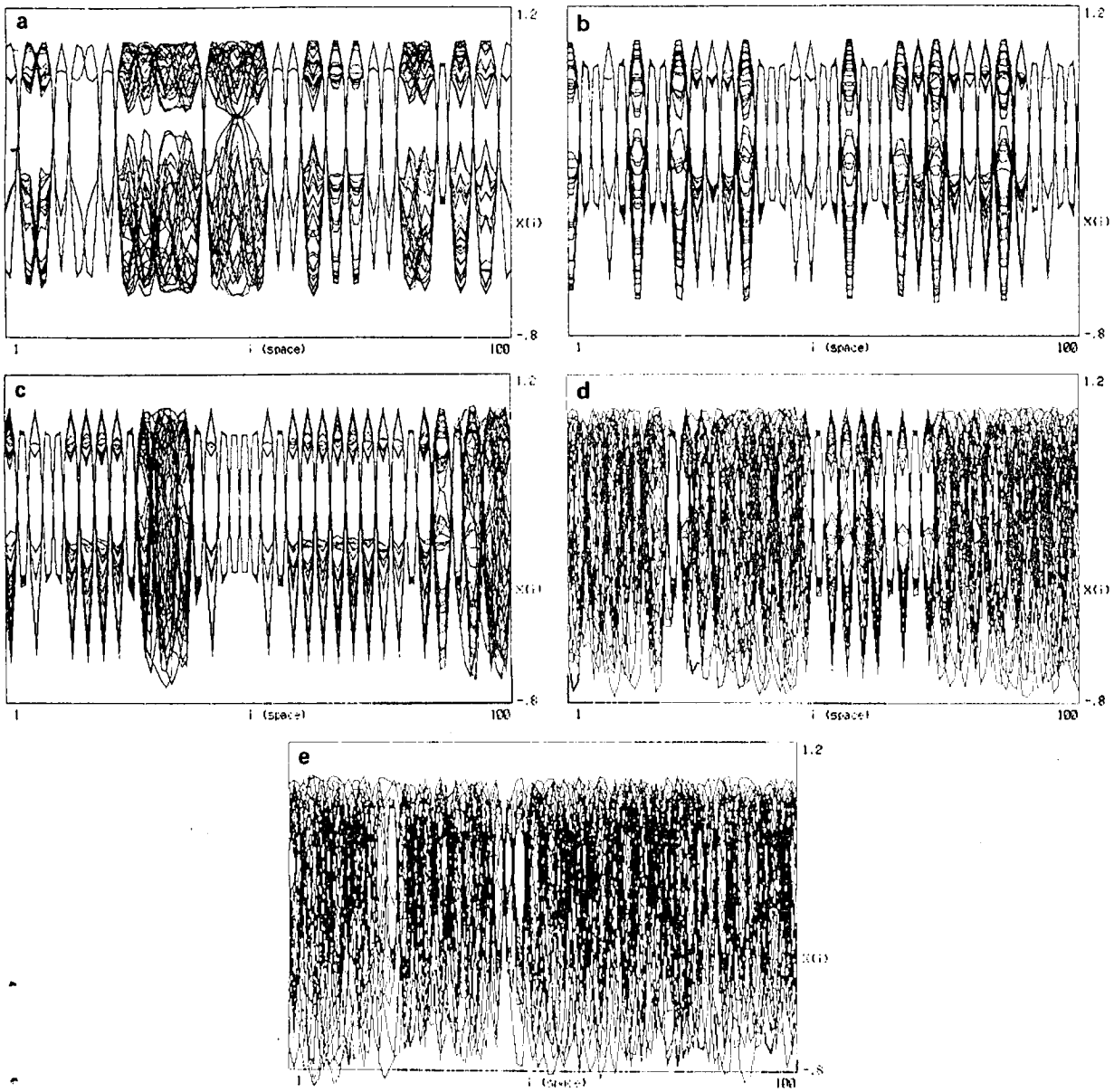

Fig. 3. Space–amplitude plot for the coupled logistic lattice (1). Amplitudes $x_n(i)$'s are overlayed for 50 time steps after the 1000 iterations of transients for the model with $\epsilon = 0.3$, $N = 100$, and random initial configurations. (a) $a = 1.48$, (b) $a = 1.56$, (c) $a = 1.68$: In (a)–(c), domain structures do not move in space. (d) $a = 1.72$, (e) $a = 1.80$.

space (see figs. 4(a) and 5(a) for the spatiotemporal diagram).

2.3. *Brownian motion of defect and defect turbulence*

As the nonlinearity is increased further, the domain boundaries start to move. Depending on the strength of the couplings, there are two phenomena associated with the motion of patterns. The first type is the diffusion of a chaotic defect [18], while the other type is the intermittency associated with the pattern competition [19].

The first one occurs in the simplest case of pattern selection, i.e., the selection of spatial mode

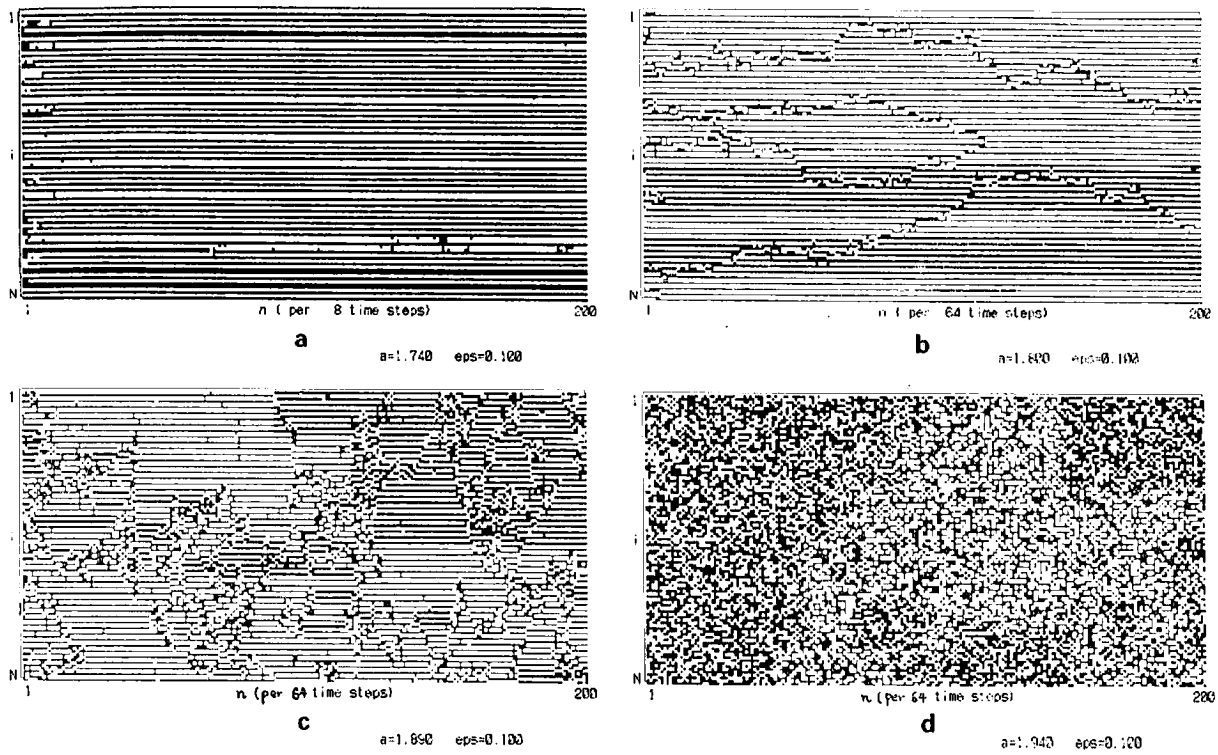

Fig. 4. Space–time diagram for the coupled logistic lattice (1), with $\epsilon = 0.1$, $N = 100$ and starting with a random initial condition. Every 8th or 64th time step is plotted from 0 to 200. If $x_n(i)$ is larger than x^* (unstable fixed point of the logistic map), the corresponding space–time pixel is painted as black, while it is left blank otherwise. (a) $a = 1.74$, (b) $a = 1.80$, (c) $a = 1.89$, (d) $a = 1.94$.

of wavelength two. The remarkable point is the existence of localized chaos as a defect which separates two domains of different phases (see fig. 2(d)). The defect is localized in space and its shape changes chaotically in time and moves around the space like a Brownian particle (see fig. 4(b)). The detailed quantitative study of the dynamics of defect will be given in section 5.

At the "defect" phase, a single zigzag state is expected to cover the whole space as time goes to infinity, since the defects pair-annihilate and are not created.

As the nonlinearity is increased further, the zigzag pattern no longer remains stable and collapses spontaneously (see figs. 2(e) and 4(c)). At the parameter close to the onset of the collapse, the zigzag region still covers a large part of the system and the state is represented as the pair-creation, pair-annihilation or multiplication of defects or generation of chaotic transients by the collisions. We term the phase as "defect turbulence", since the global turbulent structure is created by the interaction of defects.

2.4. *Pattern competition intermittency*

If the coupling is larger, the selected pattern is not unique, as can be seen in figs. 3(b, c). With the increase of nonlinearity, there appears the intermittent bursts, which have a nonstationary nature (see figs. 3(d)). The burst arises from the mismatching of phases and has much larger structures than a chaotic defect. The phase transition via this intermittency is investigated in section 6.

Strictly speaking, there are neither "defect turbulence *phase*" nor "intermittency *phase*", since these "phases" are just transition regimes between pattern selection and fully developed turbulence.

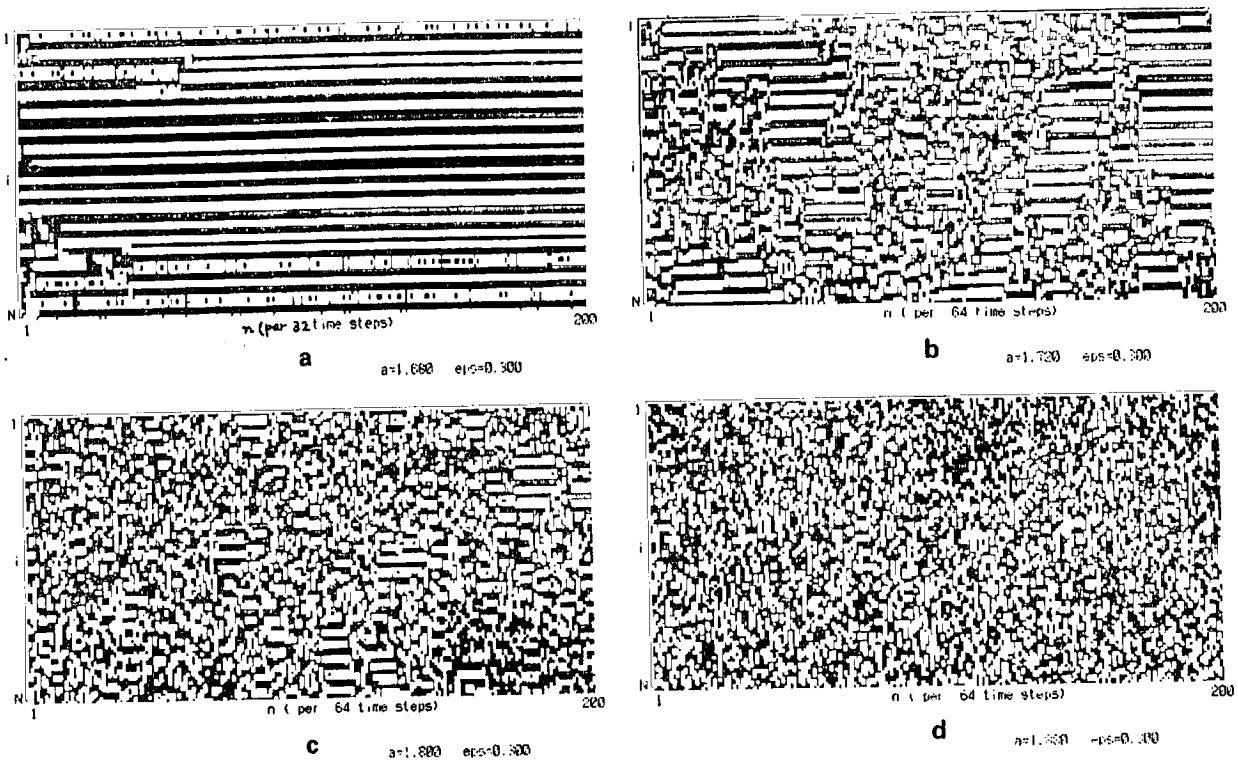

Fig. 5. Space–time diagram for the coupled logistic lattice (1), with $\epsilon = 0.3$. Every 32nd or 64th time step is plotted from 0 to 200. See caption of fig. 4 for other conditions and the method of visualization. (a) $a = 1.68$, (b) $a = 1.72$, (c) $a = 1.80$, (d) $a = 1.88$.

The reason why we put names on these regimes is that these critical regions are rather wide in a parameter space and it is of importance to study the critical behavior there in detail.

2.5. *Fully developed turbulence*

As the nonlinearity is increased further, the ordered structure in the space–time diagram can hardly be observed (see figs. 3(e) and 4(d)). The collapse of pattern with the increase of a is seen in the successive figs. 5(b–d). We call this state "fully developed turbulence" in our lattice system, since this state can be well approximated by the direct product state of local chaos with a rapid decay of spatial correlation. The state can be represented by smooth statistical and dynamical quantifiers as will be seen in the following sections. As for the conflict between the two tendencies (ordering by diffusion and inhomogenization by local chaos), the chaotic part exceeds in the ordering process in this phase.

2.6. *Phase diagram*

Let us look back at the rough phase diagram (fig. 1). The phase diagram is obtained through the simulation of the model for the parameters $a = 1.5$, $1.51, \ldots, 1.99$ and $\epsilon = 0.02, 0.04, 0.06, \ldots, 0.4$. The check of the phase is carried out by the space–time diagram, space amplitude plots, and the pattern dynamical quantifiers to be introduced later. In the diagram, "1, 2" means the pattern selection of domain size 1 or 2, and "1, 2, 3" for the pattern of domain sizes 1, 2, 3 and so on. If the size of the character "1" is larger than "2", the selected pattern consists mostly of the size 1 and has small ratio of the domain size 2. The simulations were carried out from random initial conditions.

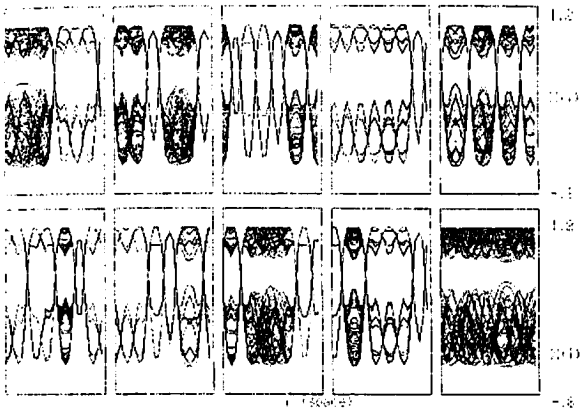

Fig. 6. Ten space–amplitude plots for the coupled logistic lattice (1), with $a = 1.5$, $\epsilon = 0.3$, and $N = 25$. Amplitudes $x_n(i)$'s are overlayed for 50 time steps after the 1000 iterations of transients. Attractors from randomly chosen 10 samples of random initial configurations are depicted. Here, domain structures do not move in space.

We note the tongue structure of selected patterns. This tongue-like structure reminds us of the locking structure in a static pattern of spatially modulated systems. The static pattern of such spatial locking structure is observed in the problems of the static configuration of some solid-state physics problems [16, 17]. The tongue structure appears as the resonance structure from the quasiperiodic state. This is essentially obtained by the replacement of time by space in the temporal resonance problem in the quasiperiodic state. Our tongue-like structure is obtained from a model both with time and space, and without free-energy-like quantities. The pattern selection in our model corresponds to the resonance structure in space. Our result shows that the spatial locking is also seen in the problem of the pattern selection in spatiotemporal chaos, if the selected pattern is fixed in space.

We also note the dominance of zigzag structures at small coupling regimes. At $\epsilon \approx 0.13$, we do not encounter the fully-developed chaos and the zigzag structure is preserved up to $a = 2$, at which the single logistic map gives the fully developed chaos. In other words, in some weak coupling regimes, the global chaos is completely suppressed.

The topics of the following sections is "how to characterize these phase changes (Frozen Random → Pattern Selection → (Defect State) → Pattern Competition Intermittency (Defect Turbulence) → Fully Developed Turbulence). Some quantifiers will be introduced to study the pattern dynamical process of our system. The characterization of each phase by these quantifiers is summarized in tables II and III, which will be explained in the following sections.

We note that this type of phase change is rather universal in the systems of local choas and diffusion. It has been observed in a large class of coupled map systems and is expected to be observed in coupled differential equation systems [20] and in partial differential equations [21]. Also, some experiments show similar phase features, as will be discussed at the end of the paper.

3. Characterization (1) (in Fourier space)

In the present and following sections, some ways of quantitative characterization of pattern dynamics of spatiotemporal chaos are briefly introduced. The results applied to our phenomena are shown along the paper.

3.1. *Spatial power spectra*

Most prevalent method for characterization of the spatial complexity is the use of Fourier transformation. The spatial power spectra are defined by

$$S(k) = \left\langle \left\langle \left| (1/N) \sum_{j=1}^{N} x_n(j)\, e^{2\pi i k j} \right|^2 \right\rangle \right\rangle, \qquad (3)$$

where $\langle\langle \ldots \rangle\rangle$ shows the long time average, although the snapshot spectra

$$s_n(k) = \left| (1/N) \sum_{j=1}^{N} x_n(j)\, e^{2\pi i k j} \right|^2, \qquad (4)$$

are useful in some cases. Some examples of the

Table II
Features of phases characterized by quantifiers (weak coupling case).

Phase \ Quantifiers	Pattern distribution function $Q(k)$	Pattern entropy S_p	Dynamical entropy S_d	Spatial power spectra	Salient features
Frozen random pattern	$Q(k) \neq 0$ for many k's	large	0	Many peaks	many attractors
Pattern selection	$Q(1), Q(2) \neq 0$ $Q(k) = 0$ otherwise	small	0	few prominent peaks	suppression of chaos
Brownian motion of defect	as time $\to \infty$ $Q(k) = \delta_{k,1}$; for a defect, $Q(k) \propto$ exp(− const. × k)	as time $\to \infty$ it goes to 0	as time $\to \infty$ it goes to 0	as time $\to \infty$ the peak at 1/2 grows	diffusion of defect triggered by chaos
Defect turbulence	$(1 - Q(1)) \propto (a - a_c)^{\beta}$	$S_p \propto (a - a_c)^{\beta'}$	$S_d \propto (a - a_c)^{\delta}$	peak at 1/2 and broad band noise at $k \approx 0$	selective flicker-like noise
Fully developed turbulence	$Q(k) \propto$ exp(− const. × k)	large	large $S_d \approx S_p$	smooth decay form $k = 0$	random pattern

Table III
Features of phases characterized by quantifiers (medium coupling case).

Phase \ Quantifiers	Pattern distribution function $Q(k)$	Pattern entropy S_p	Dynamical entropy S_d	Spatial power spectra	Salient features
Frozen random pattern	$Q(k) \neq 0$ for many k's	large	0	many peaks	many attractors
Pattern selection	$Q(p_1), Q(p_2) \neq 0$ $Q(k) = 0$ otherwise	small	0	few prominent peaks	suppression of chaos
Pattern competition intermittency	$(1 - (Q(p_1) + Q(p_2))$ $\propto (a - a_c)^{\beta}$	$S_p \propto (a - a_c)^{\beta'}$	$S_d \propto (a - a_c)^{\delta}$	few peaks and broad band noise at $k \approx 0$	selective flicker-like noise
Fully developed turbulence	$Q(k) \propto$ exp(− const. × k)	large	large $S_d \approx S_p$	smooth decay form $k = 0$	random pattern

spatial power-spectra are shown in figs. 7 (for $\epsilon = 0.1$) and 8 (for $\epsilon = 0.3$).

We note the following change of spatial power spectra with the increase of nonlinearity.

i) Slowly decaying spectra (exp(− const. × k)) with peaks at the glassy phase: Since various sizes of domains are allowed, the spatial power spectra are composed of various possible peaks (figs. 7(a) and 8(a)).

ii) Few number of sharp peaks at $k = k_{p1}$, $k = k_{p2}$, and so on are prominent by the pattern selection: The sharp peaks are located at the wavenumbers corresponding to the sizes of selected domains. As are seen in figs. 7(b,c) and 8(b–d), the number of the sharp peaks gets fewer as the selection proceeds. The peak at $k = 1/2$ is prominent at $1.75 < a < 1.88$ for $\epsilon = 0.1$ (see figs. 7(b,c)), while the peaks at $k = k_{p1} = 2/11$ and $k_{p2} = 1/6$ are shaper for $\epsilon = 0.3$, as can be seen in figs. 8(b–d).

iii) Coexistence of the peak at $k = 1/2$ and the broad band noise at $k \approx 0$ for the defect phase: As time passes the amplitude of broad band noise decrease, and finally only the peak at $k = 1/2$ remains. The broad band noise is due to the chaotic defect.

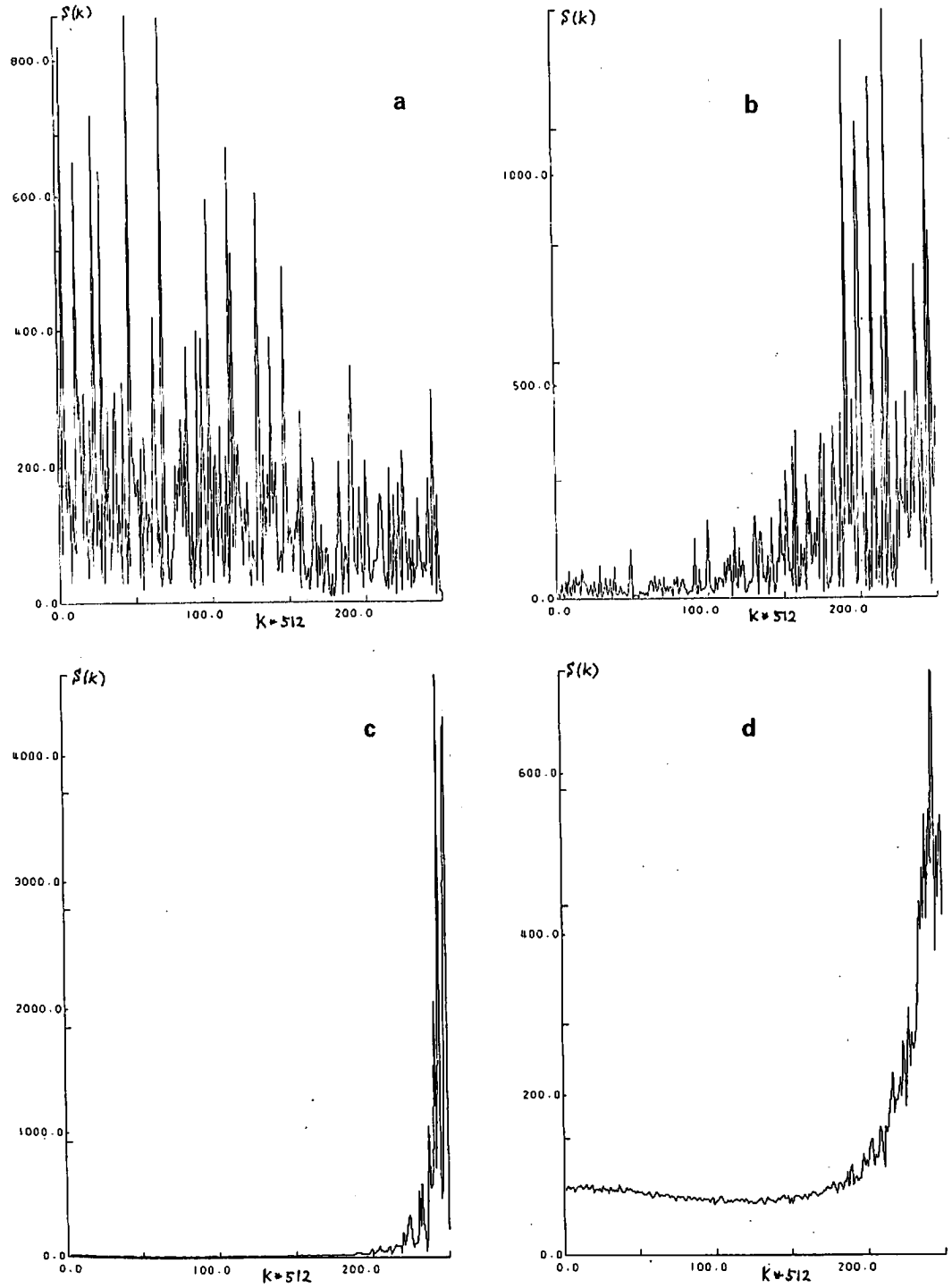

Fig. 7. Spatial power spectra $S(k)$ for the model (1), with $\epsilon = 0.1$, $N = 512$, and starting with a random initial condition. Calculated from 1000 time step averages after discarding 10000 transients. (a) $a = 1.55$, (b) $a = 1.7$, (c) $a = 1.8$, (d) $a = 1.9$.

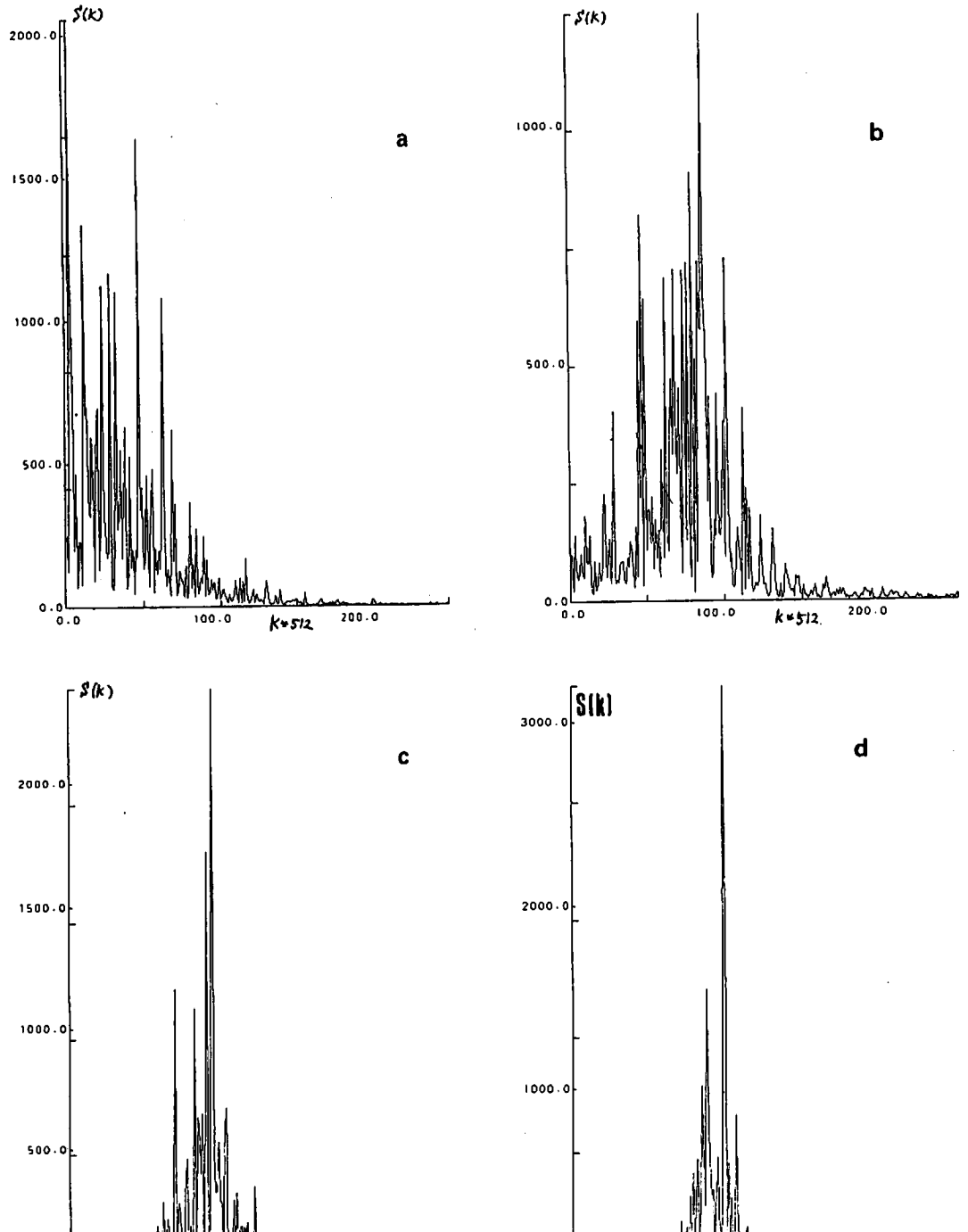

Fig. 8. Spatial power spectra $S(k)$ for the model with $\epsilon = 0.3$. See caption of fig. 7 for other details. (a) $a = 1.55$, (b) $a = 1.6$, (c) $a = 1.65$, (d) $a = 1.7$, (e) $a = 1.75$, (f) $a = 1.8$, (g) $a = 1.85$, (h) $a = 1.95$.

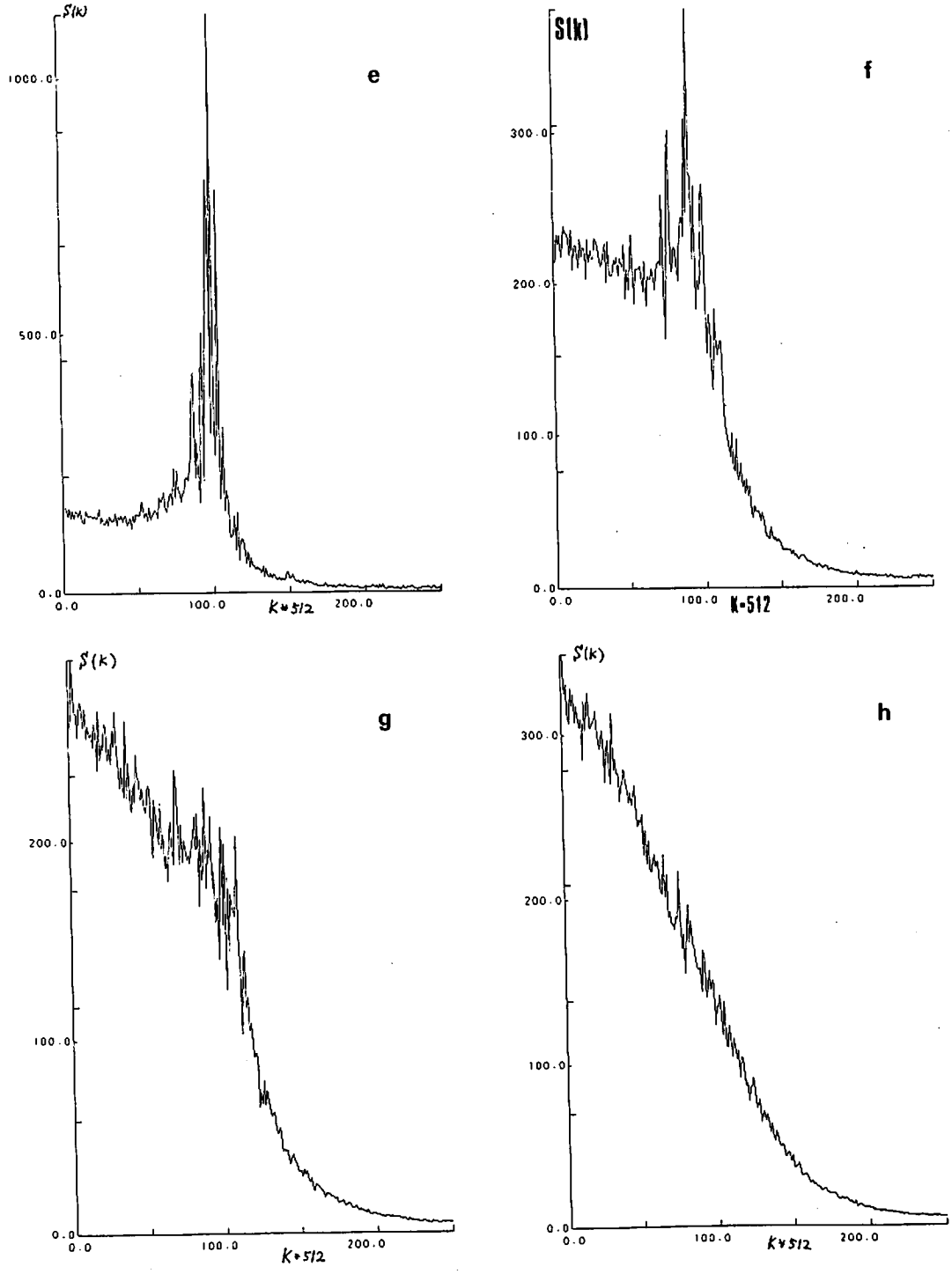

Fig. 8. Continued.

iv) Coexistence of the sharp peak(s) and the broadband noise at $k \approx 0$ for the defect turbulence or the pattern competition intermittency: In the defect turbulence, the peak at $k = 1/2$ and the broad band noise around $k = 0$ coexist (fig. 7(d)). The latter part, corresponding to the chaotic defect, increases as the nonlinearity is increased. In the intermittency case also, the burst brings about the broad band spectra at $k = 0$ for $S(k)$. The whole spectra are composed of the broad-band and the sharp peaks at the wavenumbers corresponding to the selected patterns. As the nonlinearity is increased, the portion of the broadband noise increases (see figs. 8(e, f)).

v) Fully developed spectra: As a is increased further, sharp peaks disappear completely (see figs. 8(g, h)). The spatial spectra decay monotonically as k. They are roughly fitted by the form of $\exp(-\text{const.} \times k^2)$. This Gaussian form arises from the diffusion kernel of our model.

3.2. *Spatiotemporal power spectra (dynamical form factor)*

Temporal power spectra have been a powerful tool for the study of temporal complexity, especially for the low-dimensional dynamical systems. In the case of spatially extended systems, power spectra in time and space are more useful, which are defined by

$$P(k,\omega) = \left\langle \left\langle \left| (1/N) \sum_{j=1}^{N} x_n(j)\, e^{2\pi i(jk - n\omega)} \right|^2 \right\rangle \right\rangle . \tag{5}$$

In the usual statistical mechanical problems, there is a scaling correspondence between k^2 and ω [22] for the diffusion problem. Although this scaling relation is applied to the fully developed chaos regime of our model, there also exist exceptional regimes in our model. As is discussed later, it is observed that $P(k, \omega)$ is Lorentzian as a function of ω at $k \approx 0$, while it gives the flicker-like noise for $k \approx k_p$ (the mode of the selected pattern) in the pattern competition intermittency problem (see [19] for the preliminary report). See fig. 18 in section 5 for examples. Even if the temporal part has a Lorentzian form, the half-width can largely change by the wavenumber.

3.3. *Window analysis*

In the zigzag pattern case, the spatial power spectra $s(0, n)$ and $s(1/2, n)$ may be regarded as ferro and antiferro order parameters in spin systems. Some dynamical features can be described by the motion of these order parameters. Here, the scaling analysis for the dynamics of the order parameter with the use of a window is discussed [19, 32].

For a general pattern dynamics problem, the following quantity is useful. Instead of taking the summation over all lattice points in (3.3), we take a partial summation only in a window, i.e.,

$$P(k,\omega) = \left\langle \left\langle \left| (1/M) \sum_{j=1}^{M} x_n(j)\, e^{2\pi i(jk - n\omega)} \right|^2 \right\rangle \right\rangle , \tag{6}$$

$j = 1, \ldots, M$ $(M < N)$. Let us focus on the power of some spectral mode $P(k, \omega)$. The spectral strength of such mode changes with the window size M. If the oscillation has some finite spatial correlation length ξ, the spectral strength decreases with the window size for $M < \xi$, and approaches a constant value for $M > \xi$. Near the critical point of the pattern competition intermittency, the spatial correlation length can be very large, and the spectral strength changes as M^b for $M < M_c$ and approaches constant for $M > M_c$. If the oscillation at ω appears as a collective motion of the wavenumber k, the exponent b can be positive as will be seen in the intermittency and defect turbulence. Through this analysis, we will see how the modes may be classified into relevant and irrelevant ones, borrowing the terminology in the phase transition studies [23].

4. Characterization(2) (in bit space and pattern space)

4.1. *Pattern distribution $Q(j)$ and pattern entropy*

Since the spacetime patch $x_n(i)$ has too much information, it is sometimes of use to reduce the information by a coarse-grained measurement of the continuous variables into some discrete states. Here we digitize a pattern as a symbol patch. We first assign $\sigma_n(i) = 0, 1, 2, \ldots, K-1$ to $x_n(i)$ according to the following rule:

$$\begin{aligned} &\sigma_n(i) = 0 \qquad \text{if } x_n(i) < X_1, \\ &\sigma_n(i) = 1 \qquad \text{if } X_1 < x_n(i) < X_2, \\ &\vdots \\ &\sigma_n(i) = K-1 \qquad \text{if } X_{K-1} < x_n(i). \end{aligned} \tag{7}$$

In the present paper we use the simplest digitization $K = 2$. The symbolization here is $\sigma_n(i) = 0$ for $x_n(i) < x^*$ and $\sigma_n(i) = 1$ for $x_n(i) > x^*$. In the domain structure we study here, each domain is separated by the separatrix of the unstable fixed point of the logistic map (1.2). Thus the characterization of pattern is carried out by choosing x^* as the value, i.e.

$$x^* = f(x^*) = (\sqrt{1+4a} - 1)/(2a). \tag{8}$$

Thus a snapshot pattern can be represented by a symbol sequence such as $0111\ldots001$, as is schematically shown in fig. 9. Most common characterization of the complexity of the symbol sequence is entropy, which will be briefly discussed in the next section.

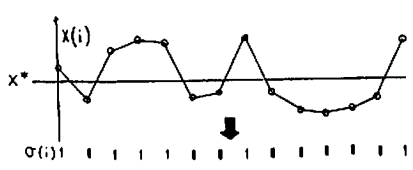

Fig. 9. Schematic representation of the coding from $x_n(i)$ to $\sigma_n(i)$.

Here we introduce a kind of order parameter for the pattern selection from the symbol sequence. The domain in section 2 is represented by the condition $(x_n(i) - x^*)$ has the same sign in the domain. Thus the probability distribution $Q(j)$ of the spatial length of the same symbol ($11\ldots11$ or $00\ldots00$) can be chosen as the order parameter(s) for our pattern dynamics. $Q(j)$ is defined by the following procedure: Take a lattice point i at a time step n: From the spatial sequence $x_n(i)$ at the fixed time n, obtain the minimum length in which $\sigma_n(k)$ takes the same symbol ($k = i-h$, $i-h+1, \ldots, i, \ldots i+m$; the length j is $h+m+1$). The length j gives the domain size of the lattice point i at the time step n. From the spatiotemporal sampling through the entire lattice and many iterations, we get the probability that a lattice point belongs to the domain of size j. For example, $Q(1) = 1$ and $Q(k) = 0$ for $k \neq 1$ for the complete zigzag pattern. In the pattern selection of two domain sizes, $Q(p_1) \neq 0$, $Q(p_2) \neq 0$ and $Q(p) = 0$ for $p \neq p_1, p_2$.

As a measure of the static complexity of pattern, we introduce the following static pattern entropy, defined by

$$S_p = -\sum_j Q(j) \log Q(j). \tag{9}$$

4.2. *Pattern transition matrix and pattern dynamical entropy*

To study the dynamics of pattern, the above quantifiers are not sufficient. We are required to construct the transition matrix of the pattern. The procedure is as follows: Take one lattice point j at a time step n and check what size of domain it belongs to (let us assume that the size of domain is m). After a given time step (we choose 8 time steps throughout the paper, but the essential part of the result is insensitive to the choice), we again calculate the size of the domain to which the lattice point belongs (let us assume it is k). This gives an event of the transition $m \to k$. By taking the spatiotemporal samplings, we obtain the prob-

ability of the transition

$T(m \to k)$ = transition from the domain with size m to that with size k. (10)

Following the dynamical entropy introduced in the study of attractors of CA by the author [24], we define a dynamical entropy of the complexity of the transition, given by

$$S_d = -\sum_{i,j} Q(i) T(i \to j) \log T(i \to j). \quad (11)$$

The meaning of the quantity is as follows; Assume that we know that a lattice point belongs to the domain of some size. After a given time step, we again observe the size of domain to which the lattice point belongs. The mutual information gain through the observation is given by S_d.

As is easily verified from the properties of the logarithmic function and the probability function, $S_p \geq S_d$ holds. If the pattern is spatially complex but temporally frozen, no transition among the domain size occurs, which leads to a positive S_p and vanishing S_d. If the transition occurs without the memory of the previous pattern (i.e., $T(i \to j) = p(j)$, independent of i), $S_p = S_d$ holds, which means that there is no dynamical ordering. The quantity S_d is especially useful in the study of the transition from frozen pattern to floating patterns.

4.3. *Lifetime distribution of pattern*

The above dynamical quantity is only applicable if the transition of patterns is represented by the Markovian dynamics. If the system has a long-time tail expressed by the $f^{-\alpha}$-type spectra, for example, the transition of pattern is not expressed by the Markovian dynamics.

To study this aspect, lifetime distribution of patterns will be calculated. The lifetime is defined as the time steps during which a lattice point remains to belong to the same domain. By taking the spatiotemporal sampling again, we get the lifetime distribution

$W_p(n)$ = the probability that a domain of size p has a lifetime n. (12)

As is expected, $W_p(n) \propto \exp(-n/t_{lf})$ for most cases, where the dynamics is represented as Markovian. The value t_{lf} is the average lifetime of the domain of the size p. If the power spectra for some patterns have the flicker-like noise, the distribution function $W_p(n)$ obeys the Pareto–Zipf form $W_k(n) \propto n^{-\Psi}$ for the corresponding domain size k, as will be seen later.

4.4. *Space–time information*

Space–time patch is taken and the entropy of possible symbol patch is calculated. See [26] for details. Let us take the patch of space length L and time interval T. The space–time entropy is defined as

$$S(L,T) = -\sum P(*) \log P(*), \quad (13)$$

where $P(*)$ is the probability of the appearance of the space–time symbol patch. Here again the coarse-graining with two symbols is often used. The data are fit by

$$S(L,T) = hLT + cL + rT + f \quad (14)$$

for large T and L. The value h corresponds to the local creation of information (KS entropy density) while the terms c and r represent the spatial and temporal flow of information respectively. The quantity represents the ratio of the abundance of the symbol patch in space–time and will characterize the complex spatiotemporal patterns in the transition sequence [26].

5. Selection of zigzag pattern and chaotic diffusion of defects

5.1. *Phenomena*

Let us investigate in detail the simplest pattern selection i.e., the selection of zigzag pattern ($k =$

1/2). Although this case is the simplest, it captures the essential aspect of pattern dynamics in spatiotemporal chaos. The zigzag pattern is easily characterized by the condition

$$(x_n(i+1) - x_n(i))(x_n(i) - x_n(i-1)) < 0 \quad (15)$$

or the condition $(x_n(i+1) - x^*)(x_n(i) - x^*) < 0$ with $x^* = (\sqrt{1+4a} - 1)/(2a)$, an unstable fixed point of the logistic map x. As was shown in section 2, the following change occurs as the increase of nonlinearity.

i) The frozen pattern: The possible domain sizes are only 1 and 2 (i.e., $Q(j) = 0$ for $j > 2$). The zigzag structure is fixed in space. The domain of size = 2 lies in the boundary of two zigzag regions. The temporal motion of the domain is chaotic (has positive Lyapunov exponents), while the zigzag region is temporally period-two.

ii) Diffusion of defect: The zigzag pattern is modulated quasiperiodically in time. The chaos in the domain boundary is still localized, but it can move in space. The defect as a domain boundary can change its size (i.e., $Q(j) \neq 0$ for $j > 2$).

iii) Diffusion of defect in chaotic media: The zigzag pattern is modulated chaotically in time, but the pattern itself is stable, i.e., the condition (15) is satisfied in the region. As for the defect, it is still localized, changes chaotically in time, and moves in space. With the increase of nonlinearity the average size of defect gradually increases.

In regions (ii) and (iii), the defects pair-annihilate and the size of zigzag regions increases with time. The system finally settles down to the completely zigzag state if the system size is even ($Q(1) = 1$, $Q(j) = 0$ for $j > 1$), while only a single defect moves around the space if N = odd.

iv) Defect turbulence: The zigzag region is no longer stable and the spontaneous pair-creation of defects in the zigzag region is seen. The turbulence as a whole consists of the interaction of defects.

v) Fully developed chaos: Almost all possible patterns are generated in a random way.

For $\epsilon = 0.1$, the phase change occurs at $a = 1.74$ ((i) → (ii)), $a = 1.83$ (ii) → (iii)), and $a = a_c = 1.88$ ((iii) → (iv)) respectively.

The spatiotemporal patterns along these phase changes can be seen in figs. 2 and 4. Another way to see the spatiotemporal dynamics is the spatial return maps [8, 5], which are the two-dimensional plots $(x_n(i), x_n(i+1))$. Some examples are given in figs. 10.

In fig. 10(a), the zigzag region and the domain of size 2 coexist and the patterns are frozen. The plots at $(x(i), x(i+1)) \approx (0.8, -0.2)$ or $(-0.2, 0.8)$ correspond to the zigzag region, while the other points close to the 4-separated curves give the motion of the domain with size = 2.

In the region (ii)–(iii), the pattern changes from the two-separated closed curves to the two-separated belt-like attractors if there is no defect, as is widely seen in the bifurcations in two-dimensional mappings. In these regimes, typical transition from torus to chaos is observed as the nonlinearity is increased (fig. 10(b–d)), i.e., lockings, and oscillation and crinkling of torus [3]. In the presence of defects, some scattered points connect the two-separated regions, which correspond to the chaotic dynamics of defects (see fig. 10(f–g) for the return maps in the presence of defects). In the fully developed regime, the spatial return map gives the folded-towel-like structures for any initial conditions, as are first found in the study of two-coupled logistic map (see fig. 10(e)) [25].

5.2. *Lyapunov spectra*

The Lyapunov spectra are calculated from the products of Jacobi matrices of the global map acting on the entire lattice. In the frozen regime, they show the stepwise structure, due to the degeneracy by the existence of separated domains [9]. In the region (ii), the initial $\sim N/3$ Lyapunov exponents are close to zero in the absence of defects (see fig. 11 (a–b)), while the spectra have positive exponents proportional to the number of defects, if there are some. In figs. 11(d–f), the Lyapunov spectra for a single defect state are shown, for N (system size) = odd. Compare fig.

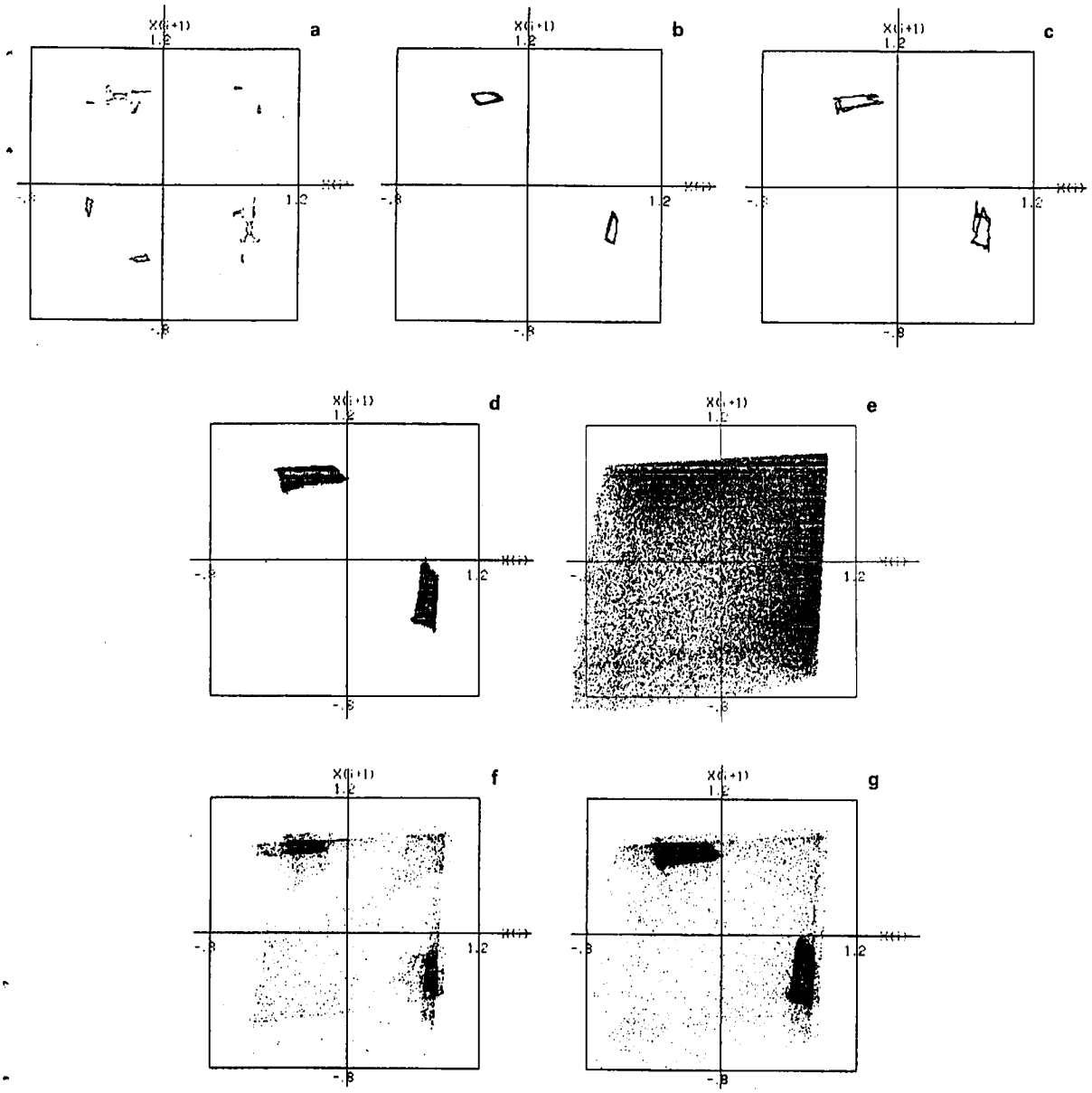

Fig. 10. Spatial return map for the model (1) with $\epsilon = 0.1$, and starting with a zigzag plus random initial condition (see eq. (16)). Points $(x_n(i), x_n(i+1))$ are plotted for the entire lattice for $1000 < n < 2000$. In figs. (a)–(e), $N = 100$. For (a)–(d), no defects exist. For figs. (f) and (g), $N = 101$ (odd) and a single defect exists. (a) $a = 1.72$, (b) $a = 1.76$, (c) $a = 1.80$, (d) $a = 1.84$, (e) $a = 1.92$, and (f) $a = 1.76$, (g) $a = 1.84$.

11(d) with (a) or 11(e) with (b). The existence of positive parts is clearly seen. This is a direct proof that a temporal evolution of defect is chaotic. We also note that the chaotic motion of defect destroys the quasiperiodic motion of zigzag structure as is seen in the spectra, which show that the exponents close to zero disappear and that they are negative now. In the region (iii), there are positive Lyapunov exponents (the number is roughly $N/2$) even in the absence of defects (fig. 11(c)). In the presence of defects, however, there are exponents which are much larger than the

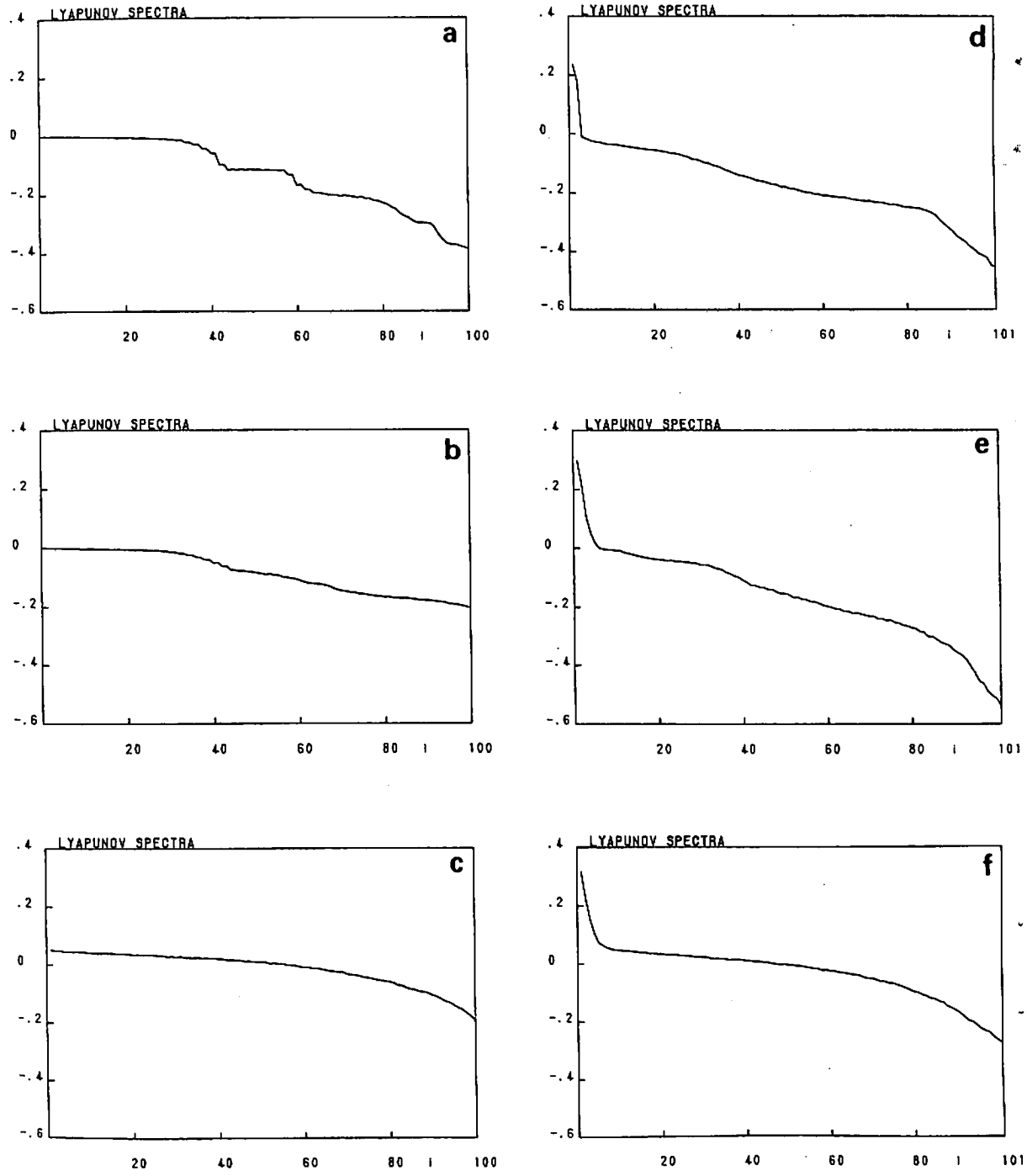

Fig. 11. Lyapunov spectra of our model with $\epsilon = .1$, starting with a zigzag initial condition (see eq. (16)). The calculation was carried out through the products of Jacobi matrices of the time steps 2000 to 5000. For (a)–(c), $N = 100$, and no defect exists, while for (d)–(f), $N = 101$ and a single defect exists. (a) $a = 1.76$, (b) $a = 1.8$, (c) $a = 1.84$ (d), $a = 1.76$, (e) $a = 1.8$, (f) $a = 1.84$.

above positive values. The number of them is proportional to the number of defects (see fig. 11(f)) for a single defect case). Thus, the chaos associated with the defect is of a different nature from the chaos in the motion of the zigzag pattern. Here again, we note that the magnitude of the other positive background exponents is decreased by the existence of defect. In other words, the chaotic motion of the background is suppressed by the existence of defect, or absorbed into the chaos of defect. In the region (iv), the spectra change smoothly as the index of exponent, which is inherent in the fully developed spatiotemporal chaos [9].

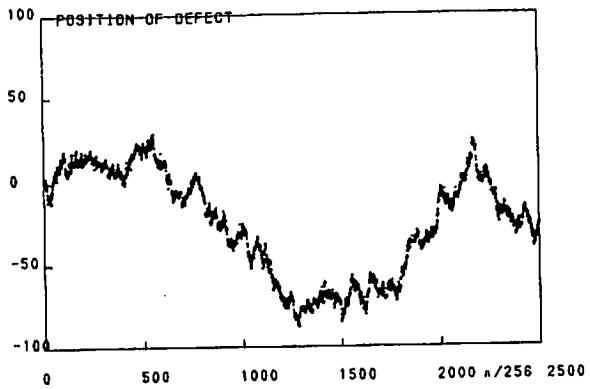

Fig. 12. Position of a defect as a function of time plotted by 256 steps for the model (1) with $a = 1.78$, $\epsilon = 0.1$, $N = 255$, and starting with a single defect initial condition (zigzag plus random as in eq. (16)).

5.3. *Diffusion coefficient of defects*

An example of the locus of the defect is given in fig. 12. It looks like the locus of Brownian particle. Here, however, it is not evident if the motion is really Brownian motion, since our system is completely deterministic. We check the property of the motion of defect in a little more detail. Note that the diffusion process here takes place *not* in the phase space (as is often discussed in the study of chaos), but in the real space [28].

In the regions (ii) and (iii), defects are not created spontaneously and they pair-annihilate by the collisions. If the motion of defect is a random walk, their number is expected to decrease as $n^{-1/2}$, with the time step n, if we start from the arbitrary chosen initial conditions. Examples of the change of number with time steps are shown in figs. 13. In the quasiperiodic regime, the decay is initially slow and may be fitted by n^{-b} with $b < 1/2$, with the time step n. This is thought to be due to the long-range correlation in the quasiperiodic zigzag region. After a larger number of iterations, however, the decay approaches $n^{-1/2}$. In the chaotic regime, the decay is rather well fitted by $n^{-1/2}$ after a few iterations.

To study the Brownian motion of the defects quantitatively in more detail, we choose a single defect initial state

$$x_n(i) = x^* + c(-1)^n + \mathrm{rnd}(b), \tag{16}$$

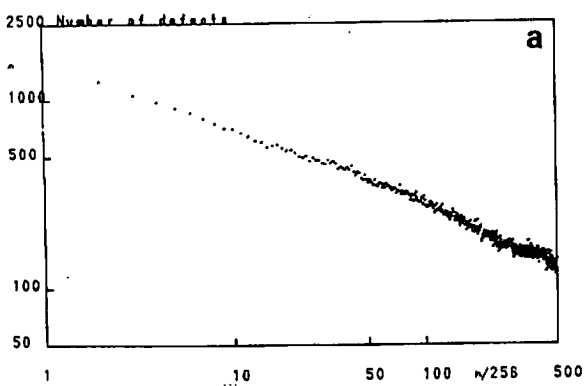

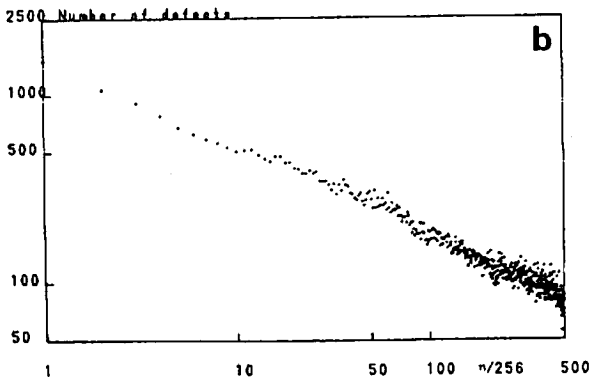

Fig. 13. Number of defects as a function of time, plotted per 256 steps, for the model (1) with $\epsilon = 0.1$, $N = 16384$ and starting with a random initial condition. (a) $a = 1.78$, (b) $a = 1.86$.

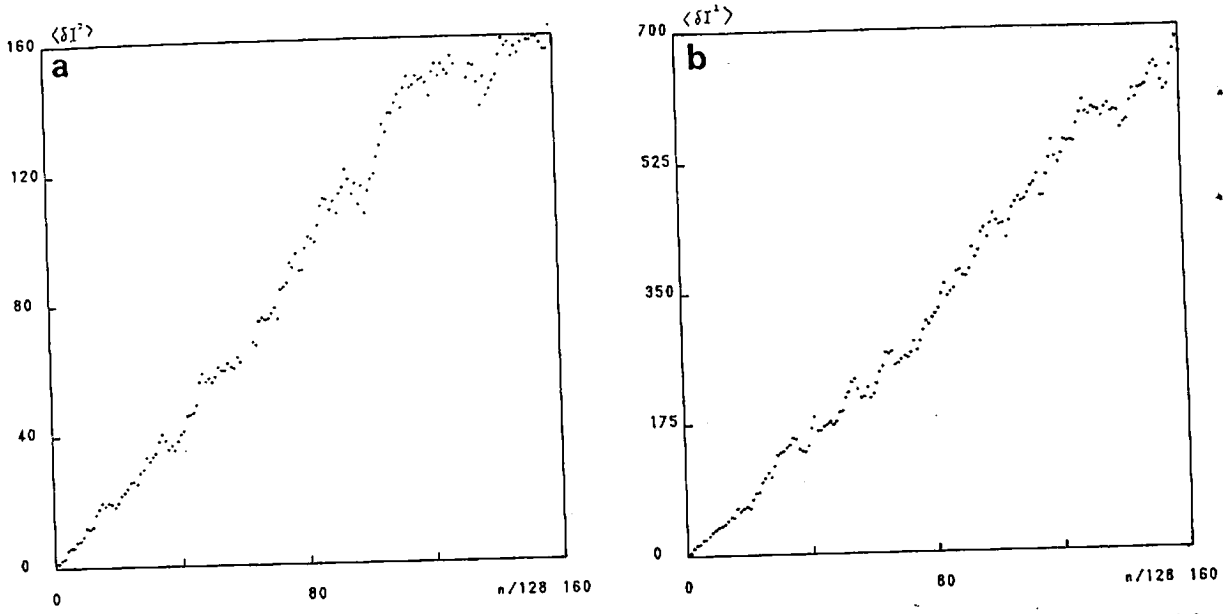

Fig. 14. $\langle (I_n - I_0)^2 \rangle$ as a function of n, plotted per 128 steps. Obtained from the sampling from 32 randomly chosen single defect states (eq. (16)), with $N = 255$, and $\epsilon = 0.1$.

where rnd(b) is a uniformly distributed random number in $(-b, b)$ and the constants c and b are chosen to generate a zigzag pattern and the system size N is an odd number (255 here) so that a single defect always exists. We calculate the position of defect I_n by the condition (15). The numerical data are fitted by the following expression:

$$\left\langle (I_n - I_0)^2 \right\rangle = 2Dn, \tag{17}$$

from which the diffusion coefficient D is calculated. Here the brackets $\langle \ldots \rangle$ represent the ensemble average for a set of initial conditions (32 samples are chosen for our calculation). The effect of periodic boundary condition is taken account of for the calculation of distance $I_n - I_0$. As can be seen in fig. 14, the fit is good both in chaotic and quasiperiodic regions.

Here we note that the random walk arises not from the randomness in the zigzag pattern, but from the chaotic motion of defect. Even if we take an almost regular zigzag initial condition ($b \to 0$ in (16)) in a quasiperiodic regime for the zigzag state, the diffusion coefficient D is the same.

The diffusion of a kink is observed in the cellular automaton problem [28], where the randomness comes from the initial random condition. Here, the important difference is that the randomness is created by the defect itself.

Numerical results for the diffusion coefficient are shown in fig. 15. We note that the logarithm of diffusion coefficient increase linearly as a both in the regions (ii) and (iii), but the slope is clearly different between the two regions.

Kolmogorov–Sinai (KS) entropy is calculated from the sum of the positive Lyapunov exponents. We take a single defect state again by taking odd number of N. KS entropy of a defect is estimated from the difference between the KS entropies of a single defect state and complete zigzag state. The logarithm of KS entropy increases linearly with a. Furthermore, the increase rate of the logarithm of KS entropy and diffusion coefficient agrees within our numerical accuracy in the region of chaotic motion of zigzag structure. This result is consistent with our guess that the diffusion is triggered by the chaotic motion of defect.

In the quasiperiodic regime, the diffusion of defect is suppressed through the long range corre-

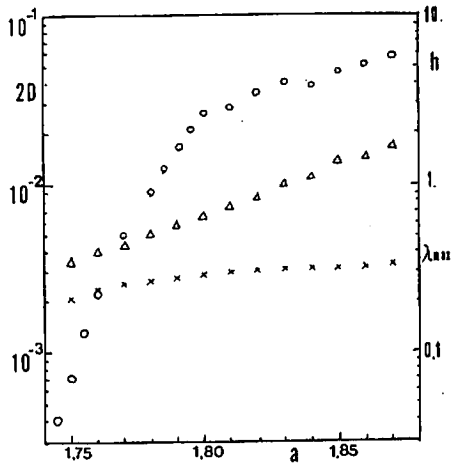

Fig. 15. Diffusion coefficient (∘), KS entropy (△), and the maximum Lyapunov exponent (×) of a defect for the model (1) with $\epsilon = 0.1$. The diffusion coefficient is calculated from the slope of the data like figs. 13, while the KS entropy is calculated from the difference of the two Lyapunov spectra with and without a defect like fig. 11. See captions of figs. 11 and 13 for detailed numerical conditions.

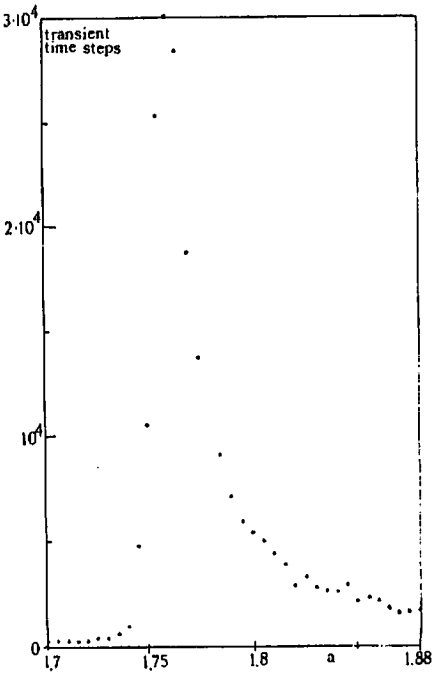

Fig. 16. Length of transients before our map (1) with $\epsilon = 0.1$ and $N = 40$ settles down into a frozen state, starting from a random initial condition. Obtained from the average over 100 randomly chosen initial conditions.

lation in the zigzag phase. We think that this is the reason why the diffusion coefficient decreases much faster than the KS entropy as the parameter a is decreased.

We also note that the maximum Lyapunov exponent of the defect changes very little within these parameter regions. The size of a defect increases more rapidly with the increase of a, which leads to the increase of the number of positive Lyapunov exponents of a defect, and to the increase of KS entropy.

Transient

In a lattice with a small size, we can check the time necessary for the disappearance of defects. This average transient time is calculated as a function of the parameter a. The result is given in fig. 16. We note the divergence at the onset of the zigzag motion, where the diffusion constant of a defect vanishes. This is not surprising, since the diffusion coefficient goes to zero there. Also, we note the divergent behavior from below the onset of diffusion. At the point $a \to a_c - 0$, the divergent behavior is not observed.

The transient length increases exponentially with a square root of the system size. Thus we can expect the existence of defects in a large system during a time interval for the usual experimental situation.

5.4. *Defect turbulence*

At $a > a_c$, the spontaneous collapse of zigzag pattern is rare and the defect picture is still valid. At these parameter regions, the dynamics is governed by the pair-creation of defects by the local crisis mechanism, their Brownian motion, and the collisions of defects, which may cause the pair-annihilation or creation of defects, or complicated transient patterns. The collision mechanism is quite similar to the "soliton turbulence" observed in coupled circle map lattices [15, 5] and some cellular automata [24, 27]. An example of space–time diagram is shown in fig. 4(c).

The phenomenon here can be understood as the crisis in a high-dimensional space (for crisis, see [29, 30]; see also [31]). As a special case, let us consider the model (1.1) with $N = 2$, i.e., a two-coupled logistic map. The map would be derived from our lattice model if the zigzag pattern were regular, i.e. $x_n(i) = x_n(i+2)$ for all i. Actually, the regular condition is not satisfied since the dynamics is chaotic and small deviation from the regular state is enhanced by the sensitive dependence of chaos. The study of two-coupled map, however, is of use as the first approximation.

The two-coupled logistic map exhibits the sudden broadening of attractor due to the crisis from the zigzag pattern at $a' = 1.92$, which is slightly larger than a_c (see figs. 17(a, b)). Toutch of the strange attractor with the stable manifolds of saddles which separate the two zigzag regions occurs at $a \approx a'$. This is quite typical in the crisis in low-dimensional dynamical systems. As the size of the system N is increased, the critical value of the collapse of the pattern decreases from a' to a_c. The value a_c is the parameter for the transition for $N = 100$ but the onset value $a_c(N)$ is converged to this value for this "large" N.

The reason of the decrease of the onset of the collapse is that the gate for the crisis is increased as the size, since the possible configuration of the deviation from the zigzag structure is enlarged. In other words, the discrepancy between a_c and a' arises from the spatially chaotic modulation of the zigzag pattern for our lattice system (1). The spatial coupling induces the propagation of the crisis to other lattice sites.

5.5. *Power spectra and window analysis*

A characteristic dynamical feature in the defect-turbulence is its long-time correlation. To study this feature, we use spatiotemporal power spectra which show the selective flicker-like noise as is seen in the present section. We first discuss the power spectrum for the whole lattice without using the window analysis. In order to remove the period-2-band like structure every other time step is taken here (x_{2n}).

In the parameter regions with defect turbulence, our system exhibits the following flicker noise for the modes with $k \approx 1/2$. In fig. 18, $P(k, \omega)$'s are plotted for $k = 0$, $2/8$, $3/8$, and $1/2$. As k approaches $1/2$, low-frequency parts grow and $P(k, \omega) = \omega^{-\alpha}$ is clearly seen for $k = k_1 (= 1/2)$. Note that the flicker noise is selectively observed only for the modes $k \approx 1/2$.

At the onset of the collapse of zigzag pattern ($a = 1.88$), α is close to 2, which means that the relaxation time diverges. As the nonlinearity parameter a is increased, the exponent α decreases from 2. The $\omega^{-\alpha}$ behavior is observed selectively for $k \approx 1/2$ at $a_c \approx 1.88 < a < 1.92 \approx a'$, although there seems to exist a plateau at $\omega \approx 0$ for $a \approx a'$. Collapse of the zigzag pattern occurs more frequently for larger a, which leads to the faster decay of correlation function and small α. Depen-

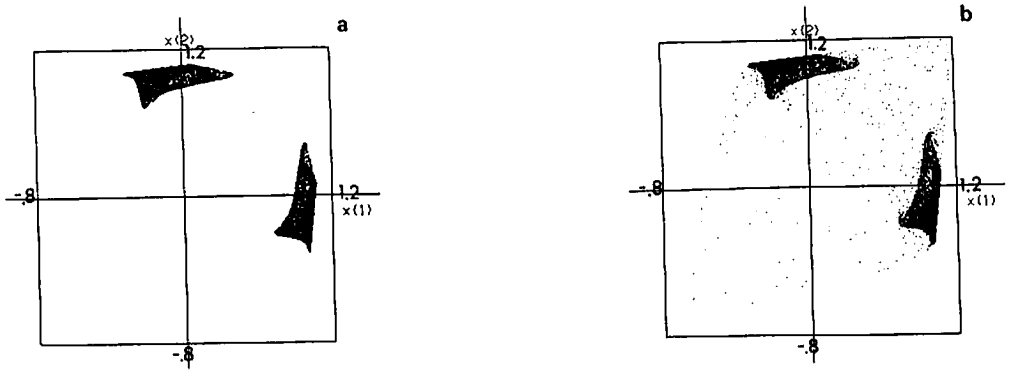

Fig. 17. Attractor for the model (1) with $\epsilon = 0.1$, and $N = 2$ (2-coupled logistic map). Points $(x_n(1), x_n(2))$ are plotted for the entire lattice for $5000 < n < 10000$. (a) $a = 1.921$, (b) $a = 1.923$.

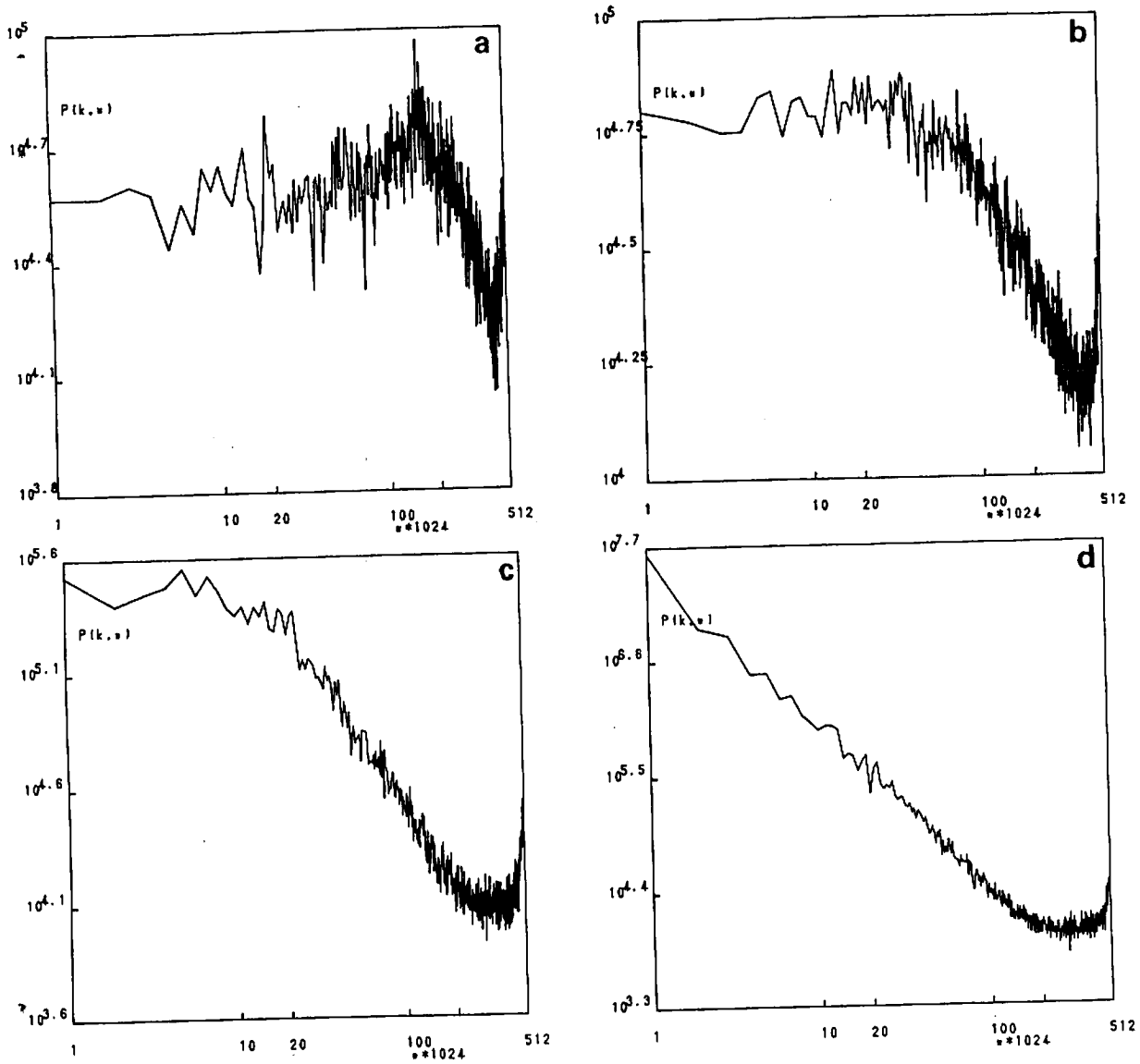

Fig. 18. Log–log plot of space–time power spectra $P(k, \omega)$ as a function of ω for $a = 1.89$, $\epsilon = 0.1$: (a) $k = 0$, (b) $k = 2/8$, (c) $k = 3/8$, (d) $k = 4/8$. These power spectra are calculated from the data of $x_{2n}(i)$ for the 512×2 time steps simulations of model (1), after 10000 steps of transients, from 50 different randomly chosen initial conditions. The system size N is 256 and the window size M is N.

dence of α on the parameter a is shown in fig. 19. For $a > a'$, the spectra have a clear plateau and the estimate of the exponent is impossible.

A possible explanation for this is that the zigzag mode exists with a long range correlation, and it is destroyed only through the long-ranged effect as is seen in the above explanation by the high-dimensional crisis in the region of $a < a'$. Thus the dynamics of the mode of wavenumber 1/2 includes the motion of very long time scale. On the other hand, the mode with $k \approx 0$ corresponds to the chaotic motion of defects, which has a short-time memory.

A reason for this critical behavior in a wide parameter regime may be attributed to the finiteness of system size. If we follow the common-sense

of phase transition, it is expected that a singular behavior is seen just at a critical point. The above power-law-type behavior in a large parameter space in a finite system, however, may be of relevance in experiments, since most "large" nonequilibrium experimental systems is substantially much smaller than those for equilibrium systems. (For example, most Bénard convection of "large" aspect ratio includes only up to 10^2 rolls.) Also, it is interesting to note that the critical behavior is easily observed in a finite system in *temporal* domain (not in spatial domain, like correlation length).

Next, we consider the change as the wavenumber k. As k is decreased from $k = 1/2$, the power decreases gradually, i.e., the mode decays in a shorter time scale. The exponent α with the change of k is shown in fig. 20, where again, plateaus at $\omega = 0$ develop as k is decreased. For smaller k, the plateaus at $\omega = 0$ appears and the spectra approach the Lorentzian form.

The flicker-like noise has been observed in a low-dimensional dynamical system at the onset of chaos through the intermittency [33, 34]. The flicker-like noise here should be noted for its selectivity to the wavenumber.

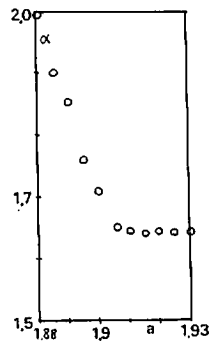

Fig. 19. Low-frequency exponent α as a function of bifurcation parameter a: The exponent α for $P(1/2, \omega) \propto \omega^{-\alpha}$ is estimated from the calculation in the same manner as in fig. 18. For $a > 1.91$, the spectra have a plateau at very low frequency ($\omega < 1/32$) and the exponent α is estimated from the data at $1/32 < \omega < 1/4$.

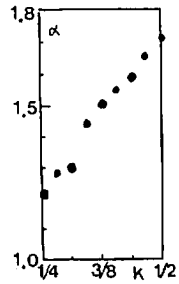

Fig. 20. Low-frequency exponent α as a function of wavenumber of k: The exponent α is estimated in the same way as in fig. 19. The system size $N = 256$. $a = 1.90$.

Window analysis

What happens if we take only a portion of our lattice system and calculate the spatiotemporal power spectra?

The selective flicker-like is still observed, although the value of the exponent α changes. As M is decreased from N, the exponent α decreases. For example, α for $M = 256$ $(= N)$, 128, 64 is ≈ 1.7, ≈ 1.5 for $M = 16$, ≈ 1.45 for $M = 8$, and ≈ 1.4 for $M = 2$ for $a = 1.90$.

Numerical results for the low-frequency spectral strength G are shown in fig. 21. Here the strength G is estimated by $\sum_{i=1}^{10} P(k, \omega = i/1024)$. We note that $G(k)$ decreases as $M^{b(k)}(b(k) < 0)$ for $k = 0$, $1/8$, $2/8$ and $3/8$ with the increase of M (e.g., $b(0) \approx -0.25$, $b(1/8) \approx -0.3$, $b(2/8) \approx -0.2$ for $a = 1.9$). The decrease stops at $M = M_c (\approx 64)$ and stays constant for $M > M_c$. On the other hand, G is increasing as M^b $(b > 0)$ for $k = 1/2$ up to $M = M_c$ (e.g., $b(1/2) \approx 0.3$ for $a = 1.9$). We note that $b(k)$ is positive only for $k \approx 1/2$, while it is negative for other modes.

The above scaling behavior is expected to hold up to $M \to \infty$ at the critical point, if we believe in the knowledge of phase transition studies in spin models. Our results near the transition show a crossover from M^b to a constant at $M \approx M_c$. If we borrow the terminology in renormalization group, the mode $k = 1/2$ may be called as relevant, while the other modes as irrelevant [23].

At $a < 1.88$, the chaotic burst corresponding to $k = 0$ is transient and a single zigzag pattern covers the whole space as $n \to \infty$. If we perform the window analysis at the transient time regime where

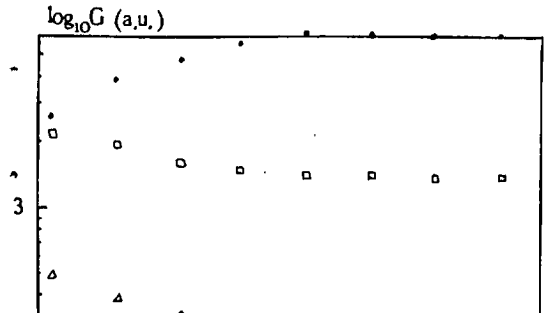

Fig. 21. The low-frequency parts of $P(k,\omega)$ with the change of window size M. $G(k) = P(k,1/256) + P(k,2/256) + \ldots + P(k,10/256)$ are plotted as a function of the window size M for the model (1) with $a = 1.895$ and $N = 256$. $\circ$ $(k = 0/8)$, $\times(k = 1/8)$, $\triangle(k = 2/8)$, $\square(k = 3/8)$, and $\bullet(k = 4/8$, scaled by $1/5)$. Arbitrary units. The power spectra are calculated in the same way as figs. 19 and 20.

the chaotic bursts still exist, M^b-behavior is observed without the crossover. For $k = 1/2$, b is positive, while it is negative for other modes. This shows the nonstationary feature of the turbulence and (ir)relevancy of modes clearly.

5.6. *Quantitative analysis of pattern dynamics*

Pattern distribution function $Q(k)$'s are useful as order parameter(s) to distinguish the different phases observed in our model. In fig. 22, $Q(k)$ for $\epsilon = 0.1$ is shown for $k \leq 5$. In the figure, only $Q(k)$'s $\neq 0$ are shown.

In the random frozen pattern, $Q(k) \neq 0$ for various k's. Furthermore, the distribution can depend on the choice of initial conditions. In the pattern selection regime, $Q(1)$ and $Q(2)$ get larger and the ratios for larger domains is suppressed $(a > 1.58)$. In the region $a > 1.64$, $Q(k) = 0$ for $k \neq 1, 2$. In these regions, the distribution can depend on the initial conditions, but the dependence is very small if we restrict to the random initial conditions and take a large N (say, > 100). Espe-

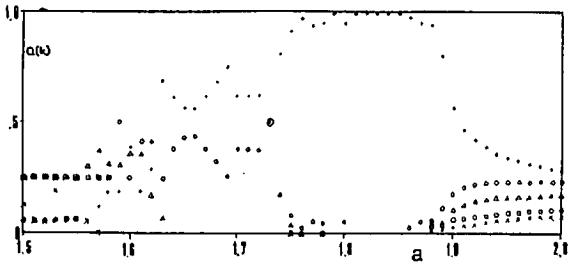

Fig. 22. Pattern distribution function $Q(k)$ $(k \leq 5)$ for the model (1) with $\epsilon = 0.1$ for $1.5 < a < 2.0$, $N = 128$ and starting with random initial conditions. $Q(k)$ is calculated from the average for 30 000 time steps after 10 000 transients. $\bullet(Q(1))$, $\circ(Q(2))$, $\triangle(Q(3))$, $\square(Q(4))$, and $\times(Q(5))$. Only $Q(k)$'s greater than 0 are shown.

cially, the selection to $k = 1$ and 2 at $a > 1.64$ is not affected by the change of initial conditions. At the defect region, it is expected that $Q(1) = 1$ and $Q(k) = 0$ for $k \neq 1$ as time goes to infinity. However, the diffusion of defect is so slow (especially in the quasiperiodic regime (ii)) that some defects still remain within the iterations of 10^4 for $N = 100$. The defect gives the distribution of

$$Q_{\mathrm{df\,c}}(k) = \left(1 - \text{const.} \times (-1)^k\right) \exp\left(-k/L_{\mathrm{df\,c}}\right) \tag{18}$$

as is shown in fig. 23. The calculation of fig. 23 is performed with the use of a single defect initial condition (5.2). The length $L_{\mathrm{df\,c}}$ gives the average size of a defect. The difference by the parity of the length k arises from the zigzag structure. The exponential decay of $Q_{\mathrm{df\,c}}(k)$ clearly indicates the localized structure of the defect. The total distribution function $Q(k)$ is given by the sum of the zigzag part $(1 - N_{\mathrm{dfc}}(n)/N)\delta_{k,1}$ and the defect part $(N_{\mathrm{dfc}}(n)/N)Q_{\mathrm{dfc}}(k)$, where $N_{\mathrm{dfc}}(n)$ is the number of defect at the time step n.

At $a > a_c$, the zigzag pattern collapses spontaneously. Thus $Q(k)$ $(k \neq 1)$ does not vanish even in the long-time limit. The value $(1 - Q(1))$ gives a measure of the destructed pattern.

Critical phenomena of the collapse of patterns are investigated through the disorder parameter $1 - Q(1)$. In fig. 24, they are shown as a function of a bifurcation parameter $a - a_c$. The data are

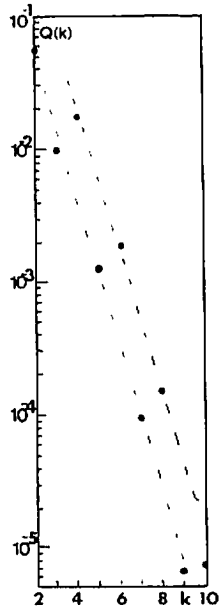

Fig. 23. Pattern distribution function $Q(k)$ for a defect for the model (1) with $a = 1.86$, $\epsilon = 0.1$, $N = 33$, and starting with zigzag initial conditions (16). Calculated from the average through 10^6 iterations after 10^4 transients. A single defect exists.

fitted roughly by

$$1 - Q(1) \approx (a - a_c)^{\beta}, \tag{19}$$

with $\beta \approx 1.0$. In the terminology of dynamical systems, these critical phenomena are explained as the crisis in a high-dimensional dynamical system. For the exponents in the crisis in low-dimensional dynamical systems, see [30], where the exponents are related with the eigenvalues of saddles.

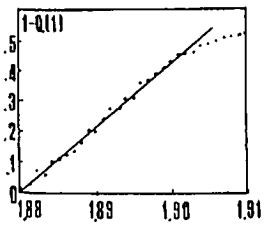

Fig. 24. Critical behavior of $1 - Q(1)$. $Q(k)$ is calculated from the average for 100000 time steps after 50 000 transients, for the model (1) with $N = 100$, $\epsilon = 0.1$ and random initial conditions.

If we change the system size from 2 to 100, the exponent β decreases from 1.6 to 1.0 (e.g., $\beta = 1.45$ for $N = 8$, 1.25 for $N = 16$). (Here, however, the determination of the onset value for the collapse is not accurate, which gives the error bars about 0.1 for the estimate of β.) The reason that the exponent decreases is that the possible pathway for the collapse is enriched by the increase of phase space of dynamical systems. The exponent at $N = 2$ is determined by the instability of the saddle, as is studied in the low-dimensional crisis, while β for $N \to \infty$ can be a statistical mechanical quantity, since the pathway in the phase space is infinite ($\mathcal{O}(N)$) dimensional. Thus the change of β with size may be regarded as a path from *the dynamical systems theory to statistical mechanical phase transition problems*.

In the fully developed regime, we note that the change of $Q(k)$'s with the bifurcation param-

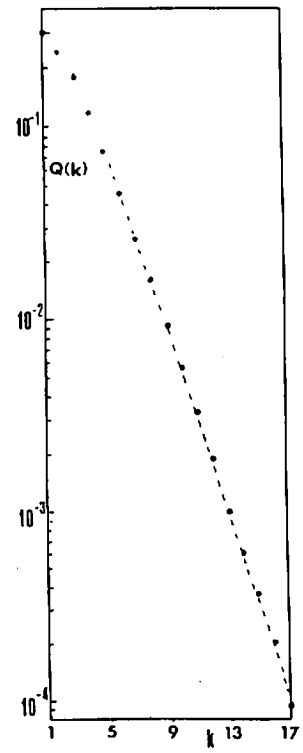

Fig. 25. Pattern distribution function $Q(k)$ for the fully developed turbulent state, calculated from the average for 30000 time steps after 50 000 transients, for our model with $a = 1.98$, $N = 128$, and $\epsilon = 0.1$.

eter is very smooth. $Q(k)$ for large k can also exist and the distribution is well fitted by $\exp(-\text{const.} \times k)$, as is shown in fig. 25. This means that the pattern dynamics is well approximated as a Markov process of 1-0 sequence. This is the reason why we call the phase as "fully developed".

A single quantity to characterize the pattern complexity is an entropy defined in section 4. The change of static pattern entropy is shown in fig. 26. The entropy is large in the frozen pattern region, and decreases rapidly by the pattern selection to zigzag state. By the pattern collapse it increases with

$$S_p \propto (a - a_c)^{\beta'}. \tag{20}$$

The exponent β' coincides with β within the numerical error as is expected, since $Q(k)$'s for $k > 1$ contributes to the increase of entropy.

The dynamical aspect of patterns is characterized by the transition matrix of patterns or (more simply) by the pattern dynamical entropy. In the frozen pattern, there is no transition among patterns, which leads to the vanishing pattern dynamical entropy, even if the static entropy is large. In the defect region, some transitions among patterns are possible if some defects remain, which give small contribution to S_d. For $n \to \infty$, this contribution decays out. At the onset of defect turbulence, the entropy increases with the form

$$S_d \propto (a - a_c)^{\delta} \tag{21}$$

with $\delta \approx \beta$ (see fig. 27). Since this exponent includes the dynamical aspect also, the equality is not obvious. Here, all we can say is that the two exponents are close numerically. At the fully developed region the difference between the dynamical and static entropies is small, which means that the transition among patterns is no more restricted and occurs randomly (see fig. 26).

In the defect turbulence region, the transition matrix cannot give a good information, since the temporal correlation has a long-time-tail and is

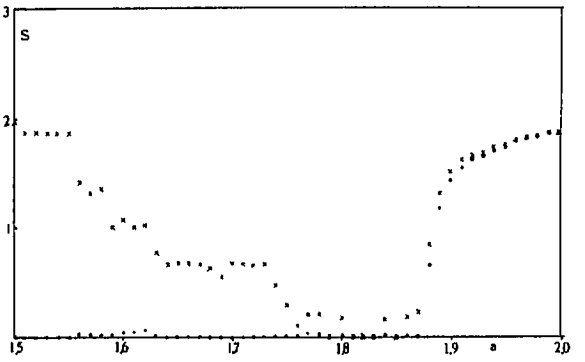

Fig. 26. Pattern (static) entropy (×) and pattern dynamical entropy (●) for our model with $\epsilon = 0.1$ and $N = 128$, calculated from the average for 30 000 time steps after 10 000 transients.

not represented by a Markovian dynamics. The lifetime distribution of zigzag pattern does not show an exponential decay but has a Pareto–Zipf form, that is,

$$W_1(n) = n^{-\psi}, \tag{22}$$

where the exponent ψ takes 1.6 for $a = 1.9$ (see fig. 28). The lifetime distribution for other patterns has a normal exponential form $W_k(n) = \exp(-n/t_{lf})$, where t_{lf} is the lifetime of the domain of size k.

The Pareto–Zipf form is typical in the dynamics with the flicker-like noise (see e.g., [33]). Since the power spectra can be written as the sum of the

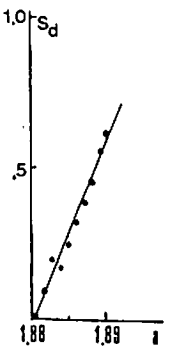

Fig. 27. Critical behavior of pattern dynamical entropy S_d, calculated from the average for 100 000 time steps after 50 000 transients, for our system $N = 100$ with $\epsilon = 0.1$ and random initial condition.

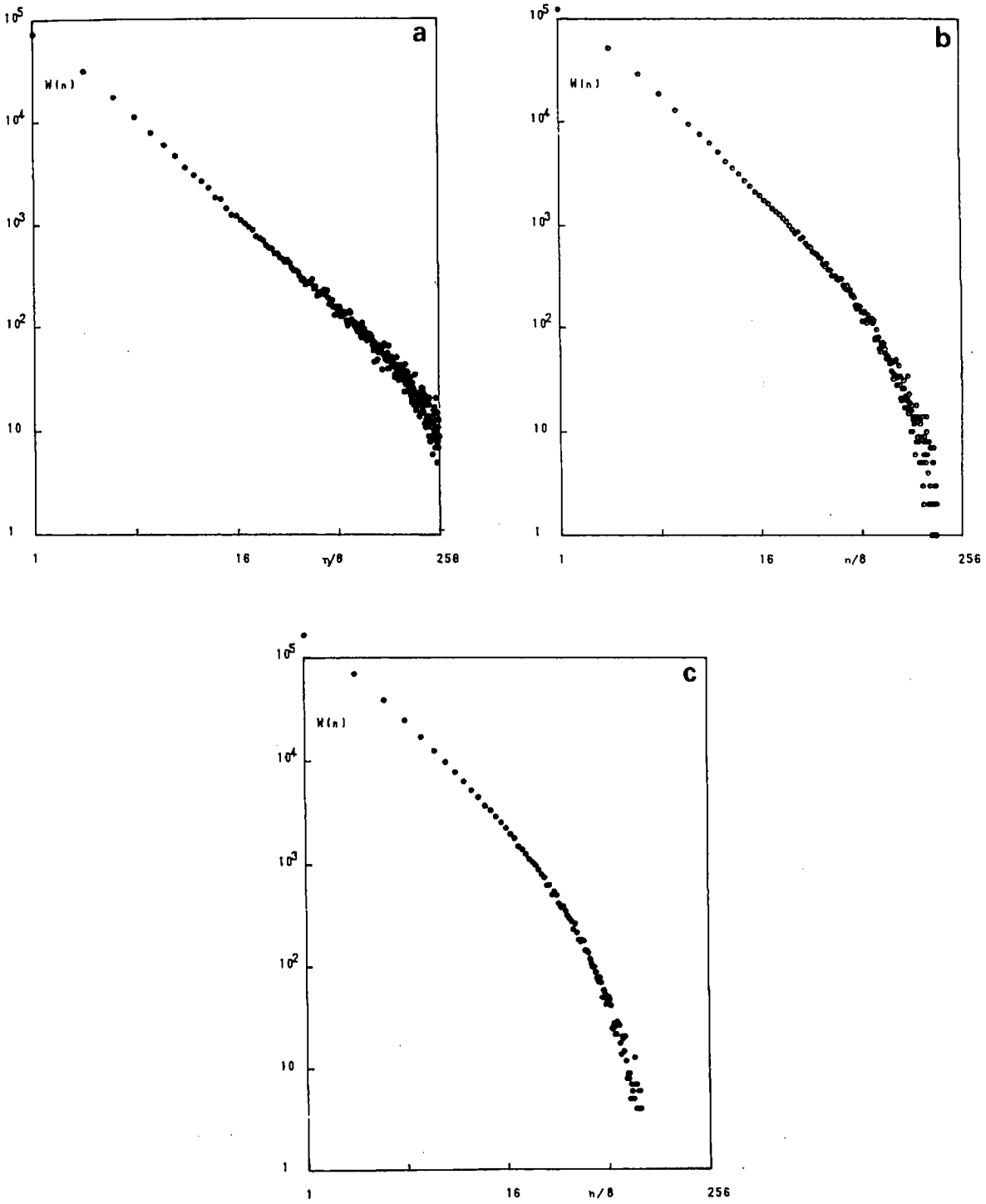

Fig. 28. Lifetime distribution $W_1(n)$ for the domain size = 1, calculated from the average for 100 000 time steps after 50 000 transients, for our model with $N = 100$, $\epsilon = 0.1$, and a random initial condition. (a) $a = 1.89$, (b) $a = 1.895$, (c) $a = 1.9$.

temporal Lorentzian form as

$$P(k,\omega) \sim \int \mathrm{d}n\, W_j(n)/(\omega^2 + 1/n^2) \qquad (23)$$

for the corresponding wavenumber k and the domain j, we can expect that the exponent ψ for domain size j and the low-frequency exponent α for the power spectra of the corresponding wavenumber ($k = 1/(2j)$) are related by

$$\psi + \alpha = 3. \qquad (24)$$

From our numerical data, $\psi + \alpha \approx 3.3$ holds. The discrepancy is due to the fact that $W_1(n)$ is a local quantity, while the exponent α is determined by the global quantity $P(k,\omega)$. Indeed, if we apply the window analysis and take a small window size for the calculation of $P(k,\omega)$, the exponent α for a small window is estimated to be 1.4 (section 5.5), which gives a consistent result with eq. (5.10).

For other parameter regions, the distribution of lifetime obeys the exponential form. The lifetime t_{lf} decreases rapidly as the increase of a in the fully-developed chaos.

Another way to estimate the lifetime is the use of transition matrix $T(i \to j)$. The lifetime for a domain of size j is proportional to $(1 - T(j \to j))^{-1}$. In the fully developed turbulence, the lifetime thus estimated decays exponentially with the size of the domain j. This is another manifestation of the random collapse of the pattern at the regime.

The main results of the section 5 are briefly summarized in table II in section 2.

6. Pattern competition intermittency

6.1. *Selection, competition, and intermittency*

The important features here are the transition sequence of (i) Frozen pattern (ii) Selection of patterns (iii) Pattern competition intermittency (iv) Fully developed turbulence. Space–time diagrams for each region are shown in fig. 5. Spatial return maps are given in fig. 29. Here the typical structure with separated regions in the return map shows the motion of selected pattern. The bursts in the intermittency connect these separated regions, as can be seen in the return maps in fig. 29.

The "pattern competition intermittency" here is characterized by the existence of more than one stable patterns and intermittent transition among patterns. Although each pattern remains to be stable by itself, the mismatch of the phases between domains makes some bursts, which move around in space–time and destroys the pattern (see fig. 5(b)). The long-range correlation in this phase is also remarkable, as will be discussed later.

The present intermittency has many aspects common with the defect turbulence in section 5. There are two different points: First, the number of selected patterns is more than one here. Sec-

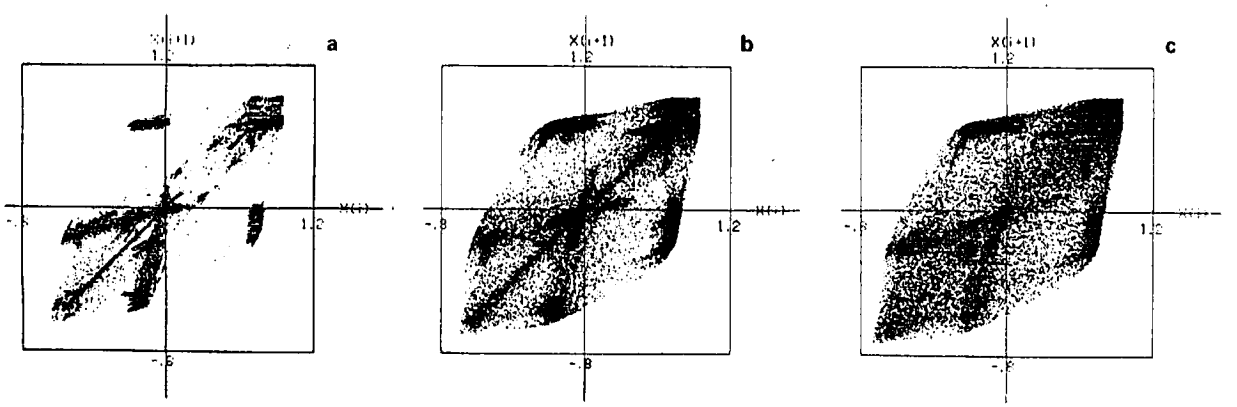

Fig. 29. Spatial return map for the model (1) with $\epsilon = 0.3$, and starting with a random initial condition. Points $(x_n(i), x_n(i+1))$ are plotted for the entire lattice for $1000 < n < 2000$. (a) $a = 1.60$, (b) $a = 1.68$, (c) $a = 1.72$.

ondly, the burst has much larger structures than the defect. This intermittency and defect turbulence belong to the spatiotemporal intermittency (STI), investigated extensively in recent years.

Here we briefly look back on STI. The STI was first studied as the spatial extension [8, 35, 5] (see also [37]) of Pomeau–Manneville's intermittency [36]. The intermittency in the present model is related with the crisis in high-dimensional systems (see also [12]). What are common in these models and the recent model by Chate and Manneville [38] is that the local dynamics has a topological chaos but non-chaotic attractor. We may conjecture that STI is seen for some coupling regimes if the local dynamics has a non-observable topological choas. (As a "local" dynamics, we may have to include the dynamics of not only one but a few sites as in the present case.)

Although STI seems to have many features common with the directed percolation [41] as suggested by Pomeau [40], the critical behavior seems to belong to a different class according to the recent investigation by Chate and Manneville [39].

The salient feature in the present intermittency with a pattern lies in its selectivity to wavenumber. This class of intermittency has first been found by [12] and may be related with the intermittency in 2-coupled logistic map [42].

One interesting feature in the intermittency phase is the existence of long-time transients. If the system size is small, the turbulent pattern can disappear by many iterations and the system finally hits the globally non-frustrated structure (see fig. 30). As the system size is increased the transient time increases rapidly (we have not yet checked the system-size dependence in detail, but it seems to increase exponentially with the system size) and for a system with $N > 100$, turbulent bursts exist at least up to within 10^5 iterations for most initial conditions.

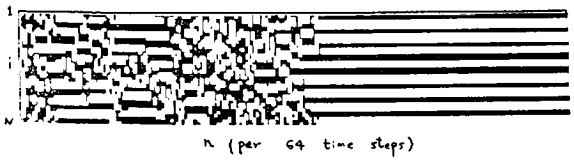

Fig. 30. Space–time diagram for the coupled logistic lattice (1), with $\epsilon = 0.3$, $a = 1.72$, $N = 40$ and starting with a random initial condition. Every 64th time step is plotted from 0 to 200. If $x_n(i)$ is larger than x^*, the corresponding space–time pixel is painted as black, while it is left blank otherwise.

In some examples it is pointed out that the weak turbulence cannot be regarded as the attractor, but the long-time transients [45]. In cellular automata, this corresponds to the class-4 rules if we follow the classification by Wolfram [2]. Another example in cellular automata is the soliton turbulence, which has been investigated by Aizawa, Nishikawa and the author [24, 27], where the turbulent phase is attributed to the transients with the length proportional to $\exp(\text{const.} \times N)$. The relevance of such class-4 CA to the dynamical system at the transition regime in the parameter space has first been pointed out by Packard and Crutchfield [43]. See also [45] for an argument on the relevance of very long transients in spatially extended systems. In the partial differential equation system, Shraiman [44] has pointed out the similar long-time transients in the pattern selection regime of the Kuramoto–Sivashinsky equation.

6.2. *Lyapunov analysis*

In fig. 31, some examples of Lyapunov spectra $\lambda(i)$ are shown. Through the Lyapunov spectra we can calculate the KS entropy density by

$$h = \sum_i{}' \lambda(i)/N, \tag{25}$$

where Σ' is the summation of positive $\lambda(i)$. The change of h with a is shown in fig. 32. Here we note the following points:

1) The stepwise structure in the spectra in the region of frozen pattern, which reflects upon the degeneracy by the existence of separated domains (see fig. 31(c)). Localized chaotic motion exists only in some large domains, which gives the positive Lyapunov exponents, the number of which is proportional to the number of such domains. Here the KS entropy increases with a.

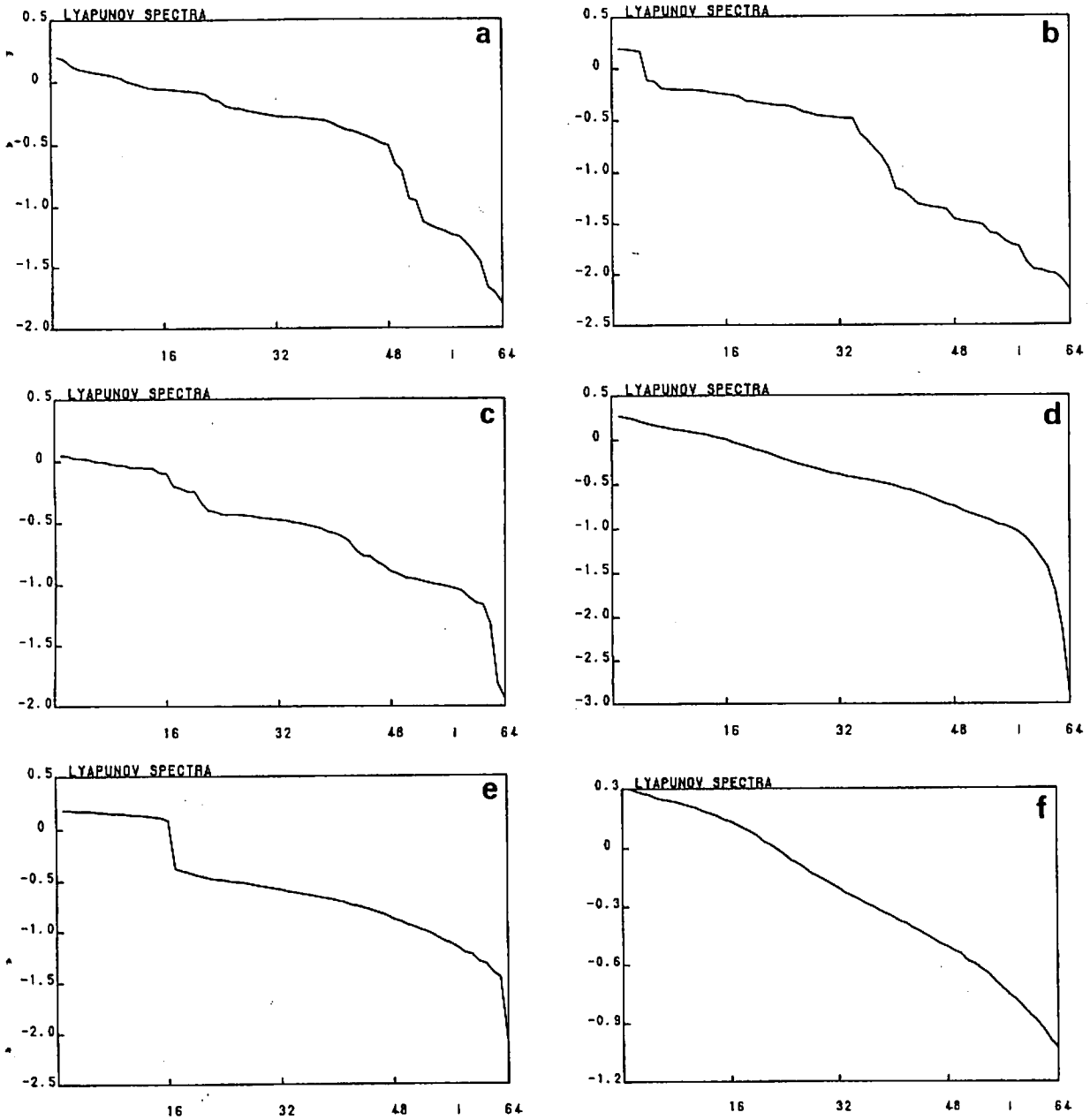

Fig. 31. Lyapunov spectra of our model with $\epsilon = 0.3$ and $N = 100$, starting with random initial condition. The calculation was carried out through the products of Jacobi matrices of the time steps 2000 to 5000. (a) $a = 1.56$, (b) $a = 1.64$, (c) $a = 1.70$, (d) $a = 1.72$, (e) $a = 1.76$, (f) $a = 1.80$.

2) The values and number of positive Lyapunov exponent decrease by the pattern selection, as is seen in fig. 31(b, c). Also, we can see that the KS entropy density in fig. 32 shows a rapid decrease at $a \approx 1.56$. These show the suppression of chaos by pattern selection clearly. The motion of selected pattern is quasiperiodic in time, which leads to the exponents close to zero (see fig. 31(c)).

3) In the intermittency region, there are some positive exponents which are not very close to zero

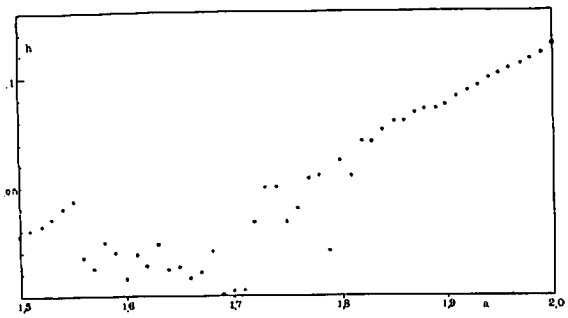

Fig. 32. KS entropy density as a function of a, calculated from the Lyapunov spectra in the same way as in fig. 31. $\epsilon = 0.3$, $N = 64$.

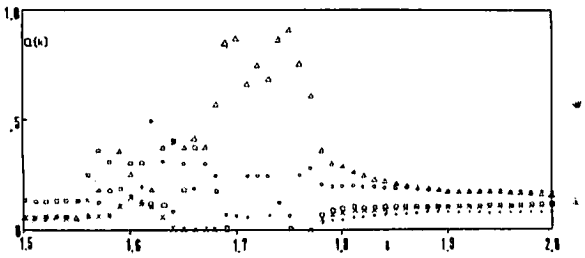

Fig. 33. Pattern distribution function $Q(k)$ for our model with $\epsilon = 0.3$ and $N = 128$, for $1.5 < a < 2.0$, and starting with random initial conditions. $Q(k)$ is calculated from the average for 3000 time steps after 5000 transients. $\bullet(Q(1))$, $\circ(Q(2))$, $\triangle(Q(3))$, $\square(Q(4))$, and $\times(Q(5))$. Only $Q(k)$'s greater than 0 are shown.

(fig. 31(d)). The stepwise structure disappears here since the burst destroys the separated domain structure. The spectra as a whole take a rather smooth shape, which is different from the spatiotemporal Pomeau–Manneville's intermittency, where the spectra are splitted to the positive and negative parts, and have a gap between the two [8].

4) In fig. 31(e), the system re-enters the region of pattern selection with frozen domains of size = 2 and 3. In the domains of size = 3, there is one chaotic mode per domain, which gives the step structure in the spectra. In the fully developed region, the spectra are smooth in form, which are close to the analytic expression for fully developed chaos in coupled-piece-wise-linear maps [9, 13].

6.3. *Power spectrum analysis*

In the pattern competition region, we have found that the flicker-like noise appears only within some limited bands of wavenumbers. Since the results are quite similar to the case of defect turbulence, we just briefly sum up them.

For $a = (1.72–1.76)$, the spectra near $k = 0$ and $k = 1/2$ obey the normal Lorentzian form, while the flicker-like noise is seen around $k = 1/6$ to $k = 1/3$ which is fit by $P(k, \omega) = \omega^{-\alpha}$. At these parameter regions, we have seen the pattern competition intermittency with the selection of domain sizes = 2 and 3. The exponent α is ≈ 1.5, for $a = 1.73$. (The dependence of α on k is small here.) The flicker-like noise is observed in rather large parameter regions.

6.4. *Quantifiers for pattern dynamics*

In the pattern competition intermittency problem, various pattern dynamical quantifiers are useful. Change of the distribution function of patterns $Q(k)$ (up to $k = 5$) with the change of a is shown in fig. 33, while the static and dynamical entropies are shown in fig. 34.

In the frozen regime, there are various possible patterns which give a large pattern entropy and a vanishing dynamical entropy. For $a > 1.55$, the selection process occurs and leads to the decrease of the pattern entropy. At $1.66 < a < 1.76$, the selection of the domain with size = 3 is clearly seen in the diagram for $Q(k)$. For $a < 1.7$, the main domain sizes are 2, 3, and 4 while for $a > 1.72$, the selection leads to the pattern only of the domains of size = 2 and 3.

In the intermittency region, the distribution $Q(k)$ consists of the domain of selected pattern (size = 2 and 3 here) and the distribution function by the burst, which has the tail of $\exp(-\text{const.} \times k)$ just like the defect turbulence case. In this region, the dynamical entropy is still very low (not zero). Through the collapse of pattern, there is a critical phenomenon similar to the case of the zigzag pattern. We can see the critical behavior of the disorder parameter $(1 - (Q(2) + Q(3)))$ and

the entropies, although detailed analysis of quantitative properties such as the determination of exponents are left for future.

In the fully developed regime, we again observe the smooth change of $Q(k)$ and entropies, and exponential decay of $Q(k)$ with k for large k. Also, the static and dynamical entropies are going closer as a is increased.

In the intermittency region, the lifetime distribution does not exhibit an exponential decay, but shows the Pareto form for the domains of size = 2 and 3, as can be seen in figs. 35(a, b) where log–log plots for $W_2(n)$ and $W_3(n)$ are depicted. Both are fitted by $W(n) \propto n^{-\psi}$ with $\psi \approx 1.75$. The exponents are the same for both domains within our numerical errors. On the other hand, the lifetime distribution obeys the usual exponential decay for other domains (see fig. 35(c) for the semi-log plot of $W_4(n)$).

Here again, sum of the exponents ψ and α gives 3.3, greater than the value required by eq. (24). The reason for this is again the same as in the defect turbulence case, and the calculation of $P(k, \omega)$ in a small window gives a smaller α and the relation (24) is restored.

The main results of the section 6 are briefly summarized in table III in section 2.

7. Summary and discussions

In the present paper, we have investigated the pattern dynamics of spatiotemporal chaos, focusing on the new phases in the spatiotemporal chaos. The salient feature of each phase is as follows: (i) Coexistence of many attractors of different patterns in frozen random phase. (ii) Suppression of chaos and the selection of a few number of patterns: we also note that the self-organization process through the transient chaos may give a new viewpoint to the traditional problem of self-organization. (iii) Brownian motion of defect triggered by its chaotic motion (iv) Selective flicker-like noise in the defect turbulence and in the pattern competition intermittency (v) Fully developed turbulence represented as the random generation of patterns. See tables II and III for a brief summary of the characterization of each phase.

We have used a synergetic approach to this pattern dynamics problem, i.e., from the viewpoints of dynamical systems theory, bifurcation theory, critical phenomena, time-series analysis, and pattern formation theory. As a dynamical system approach, Lyapunov analysis is performed and the relation with KS entropy and diffusion coefficient of defect is suggested. The shape of the Lyapunov spectra for each phase is classified. As a bifurcation theory problem, it is suggested that a collapse of pattern is due to the crisis in a high-dimensional phase space.

As a critical phenomenon, a set of pattern order parameters is introduced. Also, introduction and rough calculation of some critical exponents are carried out. Here, dynamical aspects also give us a novel interesting problem, both for the critical phenomena and time-series analysis as is seen in the discovery of the selective flicker-like noise and the window analysis for it.

Results of quantitative characterization of each phase is summarized in tables II–III.

Since the main purpose of the present paper is to illustrate a possible synthetic approach towards a novel pattern dynamics phenomenon, some remaining associated problems are listed for the future.

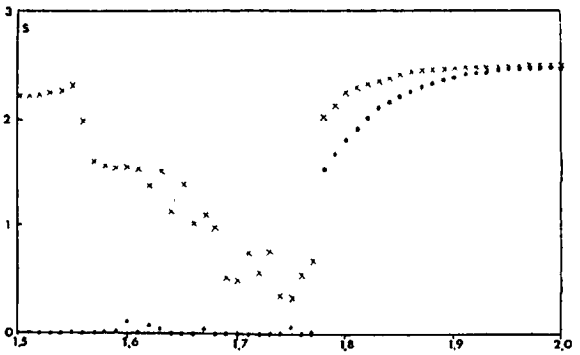

Fig. 34. Pattern (static) entropy (×) and pattern dynamical entropy (●) for our model with $\epsilon = 0.3$ and $N = 128$, calculated from the average for 30 000 time steps after 10 000 transients.

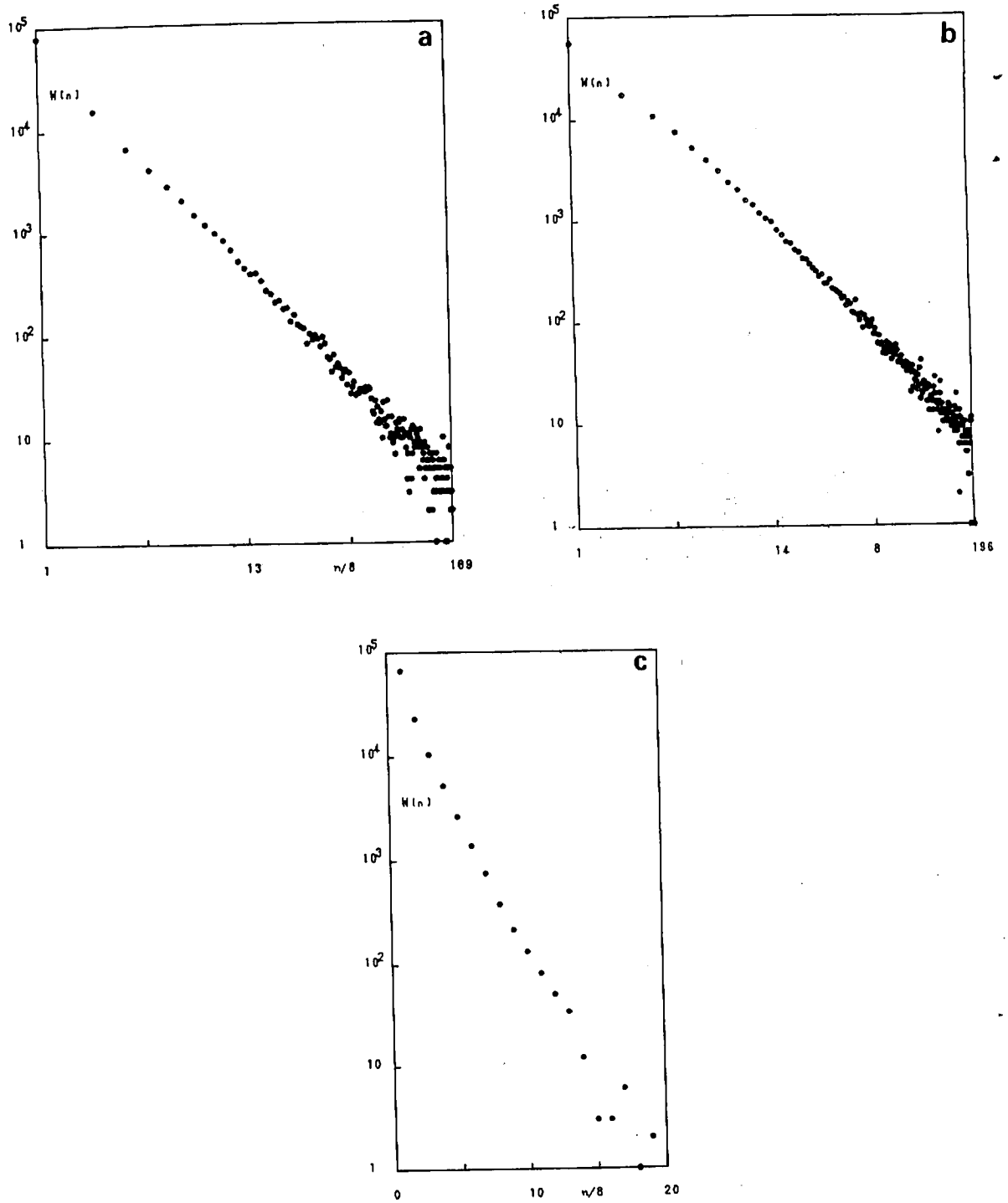

Fig. 35. Lifetime distribution $W_k(n)$, calculated from the average for 100 000 time steps after 50 000 transients, for our model with $N = 100$, $a = 1.76$, $\epsilon = 0.3$, and random initial condition. (a) $k = 2$ (log–log plots), (b) $k = 3$ (log–log plots), (c) $k = 4$ (semi-log plots).

7.1. *Critical phenomena*

The present paper has shown an example that the transition from weak turbulent state to fully developed turbulence is treated as critical phenomena. Although some quantifiers are introduced, we have neither scaling argument nor renormalization group approach for them. Construction of this approach will be a challenging problem both for the theory of turbulence and of critical phenomena. In the low-dimensional dynamical systems, the critical phenomena are related with the crisis and depend on the character of the saddle [30]. With the increase of degrees of freedom, possible paths in the phase space increase. In the limit of high-dimensional dynamical system, we may hope that the critical property is obtained by some statistical mechanical argument based on the replacement of high-dimensional dynamical systems by some stochastic motion. This, if successful, gives an example of a *pathway from dynamical systems to statistical mechanics*. Also, if this is the case, the critical property may be independent of the choice of the model within a domain of "universality class".

As for the dynamical critical phenomena, the observed selective flicker-like noise in the transition region will require a new theoretical framework.

7.2. *Fully developed turbulence and synthesis of Landau and Ruelle–Takens' pictures*

There have been two wide-spreading explanations on the turbulence. One is Landau's picture [46] which regards the turbulence as a quasiperiodic motion of infinite incommensurate frequencies. One problem for this is that it is structurally unstable and furthermore, the state seems to have very small (possibly zero) measure in the phase space. The other is Ruelle–Takens' picture [47] which regards the turbulence as a strange attractor. This has mostly been successful if the number of relevant modes is small. The low-dimensional stage attractor, however, is again structurally unstable. On the other hand, the observed fully developed turbulent state in our model (and also possibly in the real fluid turbulence) seems to be structurally stable. Indeed, in our model, windows in the original logistic map are wiped out for most initial conditions. Also, the quantifiers we have investigated are approximated by a simple Markov process, and their dependence on the bifurcation parameter is smooth. The dynamics of our system is approximated by $x_{n+1}(i) = f(x_n(i)) + \mathrm{rnd}_n(i)$, where $\mathrm{rnd}_n(i)$ is a random noise with a short memory in space and time. The noise term is strong enough to destroy the windows in the original map. These observations suggest that this state is understood as a synthesis of Landau's and Ruelle–Takens' pictures for turbulence, that is, as a direct product state of low-dimensional chaos. This picture may lead to the existence of a simple and smooth measure based on the ergodic assumption. Theoretical approach towards this direction is essential in future.

Another viewpoint for this is the synthesis of the approaches to complexity from chaos and CA. The former gives an explanation for the creation of information in the bit space [48], while the latter gives the information mixing in the real space [2]. Statistical mechanics theory is proposed for both of the systems [49–51]. Synthesis of these approaches will be required for the understanding of the fully developed turbulence in our system.

7.3. *Intermittency, defect, and transient turbulence*

Another remaining problem is a theoretical background for the transient turbulence. Some examples show the existence of turbulence not as an attractor but as a transient whose length diverges as a system size, as can be seen in the defect phase and pattern competition intermittency. Our examples and also some other numerical examples in spatially extended systems show that this is rather general, although at the present stage we have no theoretical approach towards the transient turbulence.

In connection with this problem, theoretical frameworks on the selective flicker-like noise, derivation of the Brownian motion of defect, defect turbulence, pattern intermittency, and on mechanism of the suppression of chaos by pattern selection will be required.

7.4. *Relation among the quantifiers*

Here, we have introduced the following quantifiers: Spatiotemporal power spectra, pattern distributions, entropies, dynamical entropies, pattern lifetime distribution, and Lyapunov exponents. The relations among the quantifiers have not yet been established, which have to be clarified in future. Also the relationship among the exponents in the quantifiers should be searched for, as is seen in the study of phase transition problems.

7.5. *Extensions*

In the present paper we have discussed only the pattern dynamics in the largest scale in a one-dimensional nearest-neighbor coupled map lattice. Some extensions are possible.

7.5.1. *Higher scale pattern dynamics*

In the present paper we have discussed a domain separated by an unstable fixed point x^*. This corresponds to the period-2 band motion. In the region near the onset of chaos ($a = 1.401\ldots$), we can see a finer scale of domains such as period-4 band, period-8 band, and so on, each of which is separated by period-2 unstable point, period-4 unstable point and so on, respectively. It is expected that we can see similar pattern dynamics of these smaller domains such as the pattern selection and intermittency and collapse of patterns. Actually, we have observed such behavior near the onset of chaos ($1.42 < a < 1.5$). The similar phenomenology to the present paper will be applicable to this pattern dynamics.

7.5.2. *Open flow*

Another interesting version of the coupled map lattices is the one-way coupling model, introduced as a model for the open fluid flow:

$$x_n(i) = (1-\epsilon) f(x_n(i)) + \epsilon f(x_n(i-1)). \qquad (26)$$

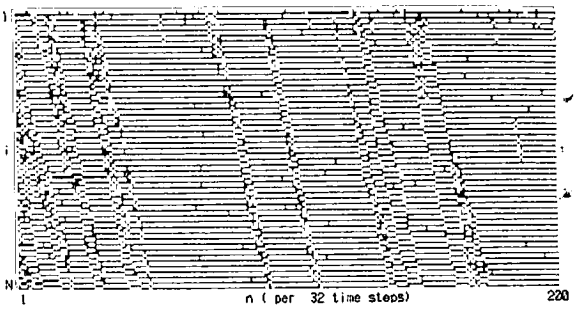

Fig. 36. Space–time diagram for the one-way coupled logistic lattice (26), with $\epsilon = 0.1$, $a = 1.82$, $N = 100$ and starting with a random initial condition. Every 32nd time step is plotted from 0 to 200. If $x_n(i)$ is larger than x^* (unstable fixed point of the logistic map), the corresponding space–time pixel is painted as black, while it is left blank otherwise.

As has already been reported [52–54], the model exhibits the spatial period-doubling and selective amplification of noise. Here we have also observed the pattern selection with some spatial wavelength and have obtained a phase diagram similar to fig. 1. We have found the defect turbulence and transmission of defect to downflow with some fluctuating velocity triggered by its chaotic motion and interaction among defects. Also, we can see a source of defect at the upper flow (see fig. 36 for an example of space–time diagram).

7.5.3. *Model with a longer range*

One might argue that the wavelength in our pattern selection is too small and the range of its change is small (as is seen in the phase diagram it is up to 4 or 5), and the behavior in our model is far from a continuous system represented by partial differential equations. The connection to the spatially smooth pattern is obtained by a simple modification of our nearest-neighbor model. First, note that our model is a repetition of the two procedures: (1) nonlinear transformation $x \to f(x)$ and (2) spatial average for a nearest-neighbor sites with the weight $(1-\epsilon), \epsilon/2, \epsilon/2$. Here the

two procedures are carried out alternately. Instead of this, we can perform D times the procedure of spatial average after every operation of the procedure (1). As is expected, this leads to a model with spatial range D and with exponentially decaying coupling strength. The result of this procedure leads to the pattern selection of much longer wavelength at the medium nonlinearity, and the transition to fully developed turbulence via the intermittency phase. Although we have not yet confirmed the quantitative details, we may hope that the model belongs to the same universality class as the present one, since in most statistical mechanical problems, nearest-neighbor and short ranged models belong to the same universality class. This modification enables us to see the connection to the continuum limit of the model in space more explicitly.

7.5.4. *Higher spatial dimension*

Extensions to higher-spatial dimensions are also of interest. We have not yet performed the detailed study, but the following features have been observed in a two-dimensional coupled map lattice:

For weak nonlinearity, selection of checkerboard-like pattern is seen [55, 15]. In our model we have observed the Brownian motion of chaotic string which separates the two antiphase checkerboard regions. We have also observed the pattern selection of longer wavelength for a stronger coupling. If the coupling is much larger, we have not yet found the selection of a longer wavelength. The intermittent transition at the collapse of pattern has also been observed.

7.6. *Possible suggestions on experiments*

To conclude the paper, we comment briefly on the possible relation of our model with experiments. First, we have to admit that the direct relation with an experiment is not possible. We do not have to be disappointed with this, however, since no direct relation with the logistic map and Rayleigh–Bénard convection is at hand in the level of equation of motion, but the map explains some aspects of the latter quite well. The key is universality. If the universality class to which our model belongs has large applicability in the spatiotemporal chaos, which we believe (since our model is so simple and general like Ising model or logistic map), we might hope that the same phenomena and quantitative aspects are observed in experiments.

What we hope to be observed is (1) the transition sequence of frozen chaotic pattern, pattern selection, intermittency (Brownian motion of defect and defect turbulence), and fully developed turbulence. If this kind of phenomena is found, the search for (2) search for selective flicker-like noise at the transition regime is recommended for a quantitative check. Also, it is desirable to reinvestigate (3) the motion of defects in some patterns, to check if the motion is chaotic, and if the Brownian motion is associated with the chaos.

Another candidate for the quantitative check will be the critical behavior of various pattern dynamical quantifiers. For a qualitative comparison, some visualization techniques introduced in the study of coupled map lattices, such as space–time diagram, spatial return maps, co-moving return maps and so on [5] may be also of use. For these qualitative and quantitative studies, multiple-point observations will be essential. Through these observations, we can get the graphics and various quantifiers comparable with those investigated in the present paper.

What are possible candidates of the experiments? We have seen some examples of spatiotemporal chaos in recent experiments [1], such as, chemical turbulence [56, 57] Bénard convection with large aspect ratio [58–62] Taylor–Couette flow with large aspect ratio [63], Faraday experiment [64] electrical convection of liquid crystal [65–67], solid state experiments such as Josephson junction array, electron–hole plasma [68], and charge density wave [69]. For open flow experiments, we have seen a lot of examples in fluid flow such as the pipeflow [70], boundary layer [71], and

air jet [72], and also in dendritic growth of crystal [73].

In these experiments, we can see some relations with our observations in the present paper. Spatial bifurcation by the frozen random state is observed in Bénard convection experiments [62]. Brownian motion of defects has been seen in the convection of liquid crystals. Localized chaotic motion (turbator) has been observed in Taylor–Couette flow [63]. Pattern competition is observed in the Faraday experiment and in liquid crystal experiment [64, 66]. Flow of turbulent spots can be frequently seen in open flow experiments and dendritic growth [73].

A remarkable experiment has recently been reported by Ciliberto and Bigazzi [74] on the Bénard convection on an annulus. The experiment exhibits the spatiotemporal intermittency which has a striking resemblance to our pattern competition intermittency in its spatiotemporal pattern, power-law distribution of laminar domains, and the existence of selected wavenumbers and of localized chaos in a subcritical region (see also [75]).

One may wonder that in most of these experiments, turbulence is induced not by local reaction term but by the spatial gradient term, as is seen in the nonlinear term of Navier–Stokes equation. In some cases, however, we expect that this is just a difference of description, and no essential difference exists. For example, let us compare the pattern selection and collapse of our model with the Bénard convection with a large aspect ratio. In the pattern selection regime, we may regard that the selected domain size corresponds to the size of Bénard cell. The turbulence in the Bénard convection triggered by the spatial coupling term between the rolls is interpreted in our model as the turbulence in the defect phase arisen from the mismatch of the two zigzag region. Thus we hope, at a level of "universality", that our prediction on the phases and the quantitative aspects is valid to these experiments, if we do not compare the global phase diagram but restrict ourselves only to each phase change. Of course, further numerical and theoretical studies are required. For these, some simulations are being performed on a coupled map models dual to the present model, i.e., trivial local dynamics and nonlinear spatial coupling terms. Some phenomena look similar, although the details will be reported in future.

Acknowledgements

The author would like to thank Y. Oono, N.H. Packard, and A. Jackson for critical reading of the manuscript and valuable comments. He would also like to thank J.P. Crutchfield, K. Ikeda, M. Sano, I. Tsuda, S. Takesue, and Y. Iba for useful discussions and critical comments. He is also grateful to Institute of Plasma Physics at Nagoya for the facility of FACOM M-380 and VP-200. This work is partially supported by the Institute of Statistical Mathematics Cooperative Research Program. This paper is based on the numerical simulations carried out in Japan, and completed at the University of Illinois. The author is thankful to the Ministry of Education of the Japanese government for financial support for the stay at Illinois and to the people at CCSR for their hospitality.

References

[1] Spatiotemporal coherence and chaos, in: Physical Systems. A.R. Bishop, G. Gruner and B. Nicholaenko, ed. (North-Holland, Amsterdam, 1986).
[2] Theory and Applications of Cellular Automata, S. Wolfram, ed. (World Scientific, Singapore, 1986).
[3] K. Kaneko, Ph.D. thesis, Collapse of tori and genesis of chaos in dissipative systems, 1983 (enlarged version is published by World Scientific, Singapore, 1986).
[4] J.P. Crutchfield, Ph.D. thesis (1983).
[5] J.P. Crutchfield and K. Kaneko, Phenomenology of spatiotemporal chaos, in: Directions in Chaos (World Scientific, Singapore, 1987).
[6] K.G. Wilson, Phys. Rev. D 10 (1974) 2445.
[7] I. Waller and R. Kapral, Phys. Rev. A 30 (1984) 2047. R. Kapral, Phys. Rev. A 31 (1985) 3868.
[8] K. Kaneko, Prog. Theor. Phys. 72 (1984) 480; 74 (1985) 1033.
[9] K. Kaneko, Physica D 23 (1986) 436.
[10] Y. Oono and S. Puri, Phys. Rev. Lett. 58 (1986) 836.

[11] T. Yamada and H. Fujisaka, Prog. Theor. Phys. 72 (1985) 885.
[12] J.D. Keeler and J.D. Farmer, Physica D 23 (1986) 413.
[13] F. Kaspar and H.G. Schuster, Phys. Lett. A 113 (1986) 451; Phys. Rev. A 36 (1987) 842.
[14] P. Alstrom and R.K. Ritala, Phys. Rev. A 35 (1987) 300. C. Tang, K. Wiesenfeld, P. Bak, S. Coppersmith and P. Littlewood, Phys. Rev. Lett. 58 (1987) 1161.
[15] K. Kaneko, Phenomenology and characterization of spatio-temporal chaos, in: Dynamical Systems and Singular Phenomena, G. Ikegami, ed. (World Scientific, Singapore, 1987).
[16] S. Aubry, in: Solitons and Condensed Matter Physics, A.R. Bishop and T. Schneider, eds. (Springer, New York, 1978).
[17] P. Bak, Rep. Prog. Phys. 45 (1982) 587.
[18] K. Kaneko, Eur. Phys. Lett. 6 (1988) 193.
[19] K. Kaneko, Phys. Lett. A 125 (1987) 25.
[20] D.K. Umberger, E. Ott and C. Grebogi (private communication) have observed the doubling of kink–antikinks and domain separation in a chain of coupled Duffing oscillators, which are quite similar to those observed in coupled logistic lattices [3–5, 8, 9].
[21] In Kuramoto–Sivashinsky equation, a similar pattern selection has been found by U. Frisch, S. Che, and O. Thual, in: Macroscopic Modelling of Turbulent Flows, U. Frisch, ed. (Springer, Berlin, 1985).
[22] See e.g., K. Kawasaki, in: Phase Transitions and Critical Phenomena, vol. 2, C. Domb and M.S. Green, eds. (Academic Press, London, 1972). P.C. Hohenberg and B.I. Halperin, Rev. Mod. Phys. 49 (1977) 435.
[23] See e.g., D.J. Amit, Field Theory, Renormalization Group and Critical Phenomena (McGraw-Hill, New York, 1978).
[24] K. Kaneko, in: Theory and Applications of Cellular Automata, S. Wolfram, ed. (World Scientific, Singapore, 1986), pp. 367–399.
[25] K. Kaneko, Prog. Theor. Phys. 69 (1983) 1477.
[26] J.P. Crutchfield and K. Kaneko, Space–time information theory, in preparation.
[27] Y. Aizawa, I. Nishikawa and K. Kaneko, in preparation.
[28] P. Grassberger, Physica D 10 (1984) 52.
[29] C. Grebogi, E. Ott and J.A. Yorke, Phys. Rev. Lett. 48 (1982) 1507; 57 (1986) 1284; Physica D 7 (1983) 181.
[30] C. Grebogi, E. Ott and J.A. Yorke, to appear in Phys. Rev. A.
[31] This high-dimensional crisis picture may be related with the homoclinic excursions in high-dimensional systems: A.C. Newell, D.A. Rand and D. Russel, preprint.
[32] For a similar approach to a discrete epidemiological model, see Y. Iba, to be published.
[33] Y. Aizawa, C. Murakami and T. Kohyama, Prog. Theor. Phys. 79 (1984) 96.
[34] I. Procaccia and H. Schuster, Phys. Rev. A 28 (1983) 1210. B.C. So, N. Yoshitake, H. Okamoto and H. Mori, J. Stat. Phys. 36 (1984) 367.
[35] See for a possible reduction to probabilistic CA, K. Kaneko, in: Dynamical Problems in Soliton Systems, S. Takeno, ed. (Springer, Berlin, 1985), pp. 272–277.
[36] Y. Pomeau and P. Manneville, Comm. Math. Phys. 74 (1980) 189.
[37] See also H. Chate and P. Manneville, C.R. Acad. Sci. 304 (1987) 609; Phys. Rev. Lett. 58 (1987) 112.
[38] H. Chate and P. Manneville, submitted to Physica D (preprint received during the revision of the present paper).
[39] H. Chate and P. Manneville, submitted to Phys. Rev. A (preprint received during the revision of the present paper).
[40] Y. Pomeau, Physica D 23 (1986) 3.
[41] S.P. Obukhov, Physica A 101 (1980) 145.
[42] T. Yamada and H. Fujisaka, preprint, to appear in Prog. Theor. Phys.
[43] N.H. Packard and J.P. Crutchfield, private communication.
[44] B.I. Shraiman, Phys. Rev. Lett. 57 (1986) 325.
[45] J.P. Crutchfield and K. Kaneko, Phys. Rev. Lett. 60 (1988) 2715.
[46] L.D. Landau and E.M. Lifshitz, Fluid Mechanics (Pergamon, London, 1959), chap. 3.
[47] D. Ruelle and F. Takens, Comm. Math. Phys. 20 (1971) 167; 23 (1971) 343.
[48] R. Shaw, Z. Naturforshung. 36a (1981) 80.
[49] R. Bowen and D. Ruelle, Inventiones Math. 29 (1975) 181. D. Ruelle, Thermodynamic Formalism (Addison Wesley, Reading, MA, 1978).
[50] Y. Oono and Y. Takahashi, Prog. Theor. Phys. 63 (1980) 1804.
[51] Y. Oono and C. Yeung, J. Stat. Phys. 48 (1987) 593. See also, Y. Oono and M. Kohmoto, Phys. Rev. Lett. 55 (1985) 2927.
[52] K. Kaneko, Phys. Lett. A 111 (1985) 321.
[53] R.J. Deissler and K. Kaneko, Phys. Lett. A 119 (1987) 397.
[54] R.J. Deissler, Phys. Lett. A 120 (1987) 334.
[55] G.L. Oppo and R. Kapral, Phys. Rev. A 33 (1986) 4219.
[56] A.T. Winfree, in: Oscillation and Travelling Waves in Chemical Systems, R.J. Fields and M. Burger, eds. (Wiley, New York, 1985). See also Y. Kuramoto, Chemical Oscillations, Waves and Turbulence (Springer, New York, 1984), for theoretical stage.
[57] H. Yamazaki, Y. Oono and K. Hirakawa, J. Phys. Soc. Jpn. 44 (1978) 335.
[58] G. Ahlers and R.P. Behringer, Prog. Theor. Phys. 64 (1978) 186.
[59] E. Moses and V. Steinberg, Phys. Rev. Lett. 57 (1986) 2018.
[60] S. Ciliberto and M.A. Rubio, Phys. Rev. Lett. 58 (1987) 2652.
[61] R.W. Walden, P. Kolodner, A. Passner and C.M. Surko, Phys. Rev. Lett. 55 (1985) 496.
[62] S. Sato, M. Sano and Y. Sawada, Phys. Rev. A 37 (1988) 1679.
[63] R.J. Donnelly et al., Phys. Rev. Lett. 44 (1980) 987. G.W. Baxter and C.D. Andereck, Phys. Rev. Lett. 57 (1986) 3046.

[64] S. Ciliberto and J.P. Gollub, Phys. Rev. Lett. 52 (1986) 922.
[65] S. Kai and K. Hirakawa, Prog. Theor. Phys. Suppl. 64 (1978) 212.
[66] M. Lowe, J.P. Gollub and T.C. Lubensky, Phys. Rev. Lett. 51 (1983) 786.
[67] S. Chandrasekhar, Adv. Phys. 35 (1981) 507.
[68] R.V. Buskirk and C.D. Jeffries, Phys. Rev. A 31 (1985) 887.
[69] A. Zettl, Physica D 23 (1986) 155.
[70] See e.g., K.R. Sreenivasan, in: Frontiers of Fluid Mechanics, S.H. Davis and J.L. Lumley, eds. (Springer, Berlin, 1985).
[71] See e.g., J.J. Riley and M. Gad-el-Hak, in: Frontiers of Fluid Mechanics, S.H. Davis and J.L. Lumley, eds. (Springer, Berlin, 1985).
[72] M. Bonetti, R. Meynart, J.P. Boon and D. Olivari, Phys. Rev. Lett. 55 (1985) 492.
[73] Y. Sawada, Physica A 140 (1986) 134.
[74] S. Ciliberto and P. Bigazzi, Phys. Rev. Lett. 60 (1988) 286 (paper published during the revision of the present manuscript).
[75] According to a recent communication during the revision of the present manuscript, S. Nasuno, M. Sano, and Y. Sawada have observed the selective flicker noise at the spatiotemporal intermittency for a two-dimensional electrical convection of liquid crystal.

Note added in proof. For recent progress in pattern dynamics in a 2-dimensional lattice and pattern selection transition, see K. Kaneko, Spatiotemporal Chaos in One- and Two-Dimensional Coupled Map Lattices, Physica D, to be published.